

Corrosion of Cellular Metals in Marine Environments

John R. Scully

Principle Investigator
Center for Electrochemical Science and Engineering
Department of Materials Science and Engineering
University of Virginia
Charlottesville, VA 22911

ONR Grant N00014-03-1-0497
Period of Performance
April 1, 2003, to August 31, 2006

For: Dr. David A. Shifler Ph.D, P.E.
Office of Naval Research
875 N. Randolph Street, Suite 1425
ONR 332, Room 631
Arlington, VA 22203-1995

Phone: (703) 696-0285
FAX: ((703) 696-0934
Email: shifled@onr.navy.mil

³⁰
September 31, 2006

DISTRIBUTION STATEMENT A
Approved for Public Release
Distribution Unlimited

TECHNICAL OBJECTIVES

The specific objective of this research is to establish the foundation to enable the next generation of corrosion resistance cellular metals for high performance naval applications. The basis for this work is an interdisciplinary approach that aims to understand: (a) the electrochemical, chemical, and metallurgical conditions that corrode cellular metals in marine environments when fabricated by brazing processes, (b) the impact of braze fabrication time, temperature and diffusion length on corrosion resistance and optimization of the same, and (c) elucidation of corrosion mechanisms so as to provide fundamental information on processes that govern corrosive attack and guide mitigation strategies whether by protection of existing braze materials or by design of new brazing materials. Specifically FY 2005 was dedicated to elucidating the corrosion mechanisms of a super-austenitic stainless steel Al-6XN (Fe-24Ni-20Cr-6.3Mo-0.22N) when brazed with a commercial Nicrobraz alloy (Nicrobraz 31: Ni-22Cr-6.3Si-3.8P).

BACKGROUND

Honeycomb core sandwich panels represent today's state of the art in ultra lightweight structure.[1-4] However, these cellular materials can be expensive to manufacture and aluminum alloy variants suffer from corrosion problems. Recently, great interest has developed in the use of other cellular metal cores in part because many, potentially low cost methods for their manufacture are being developed.[5-6] Their mechanical performance depends upon the topology of the cells, and so it is useful to classify cellular metals by the size of their cells, their cell type (open or closed) and their relative density.

Corrosion is a major concern for any ultra-light cellular metal core sandwich panels exposed to salt water environments.[7] Many of the attributes of lightweight cellular metal concepts dictate the need for fabrication using corrosion resistant materials (CRMs) possessing *intrinsic* corrosion resistance. Examples of weight-savings attributes in cellular metals that necessitate the use of CRMs include the finite thickness of the sandwich face sheets that limits tolerance to corrosion initiation and eliminates any "allowable corrosion damage" as well as the cellular metal core region containing many occluded sites. Moreover, corrosion *allowance* materials that lack *intrinsic* corrosion resistance are impractical because of the difficulty in insuring essential and long lasting corrosion protection to both exposed surfaces and in occluded regions. Thus, attributes of cellular metal concepts dictate that CRMs capable of maintaining *intrinsic* passivity in corrosive environments as well as resisting several forms of local corrosion be considered. Hence, stainless steel, Ni-base alloys and titanium alloys with *intrinsic* corrosion resistance are desirable candidates, amongst others for Marine applications. The choice of a superaustenitic stainless steel can provide good corrosion resistance in seawater environments and provide a cost effective material with the necessary intrinsic resistance.[8-11] Maintaining good corrosion resistance by using materials that possess intrinsic corrosion resistance in various ultra-lightweight cellular metal concepts such as metal textile, honeycomb and truss-core concepts will also depend critically on geometry, environment severity, material and bond method.

Facesheet to core bonding presents a critical corrosion issue. A concern with welded, brazed or transiently liquid metal bonded construction of lightweight sandwich structures with CRMs, given possible exposure to marine type saline environments, is the *altered* metallurgical condition of the base material and the introduction of a new material with a different composition and structure associated with the bonded region between the core material and the face sheet. At

issue is both the corrosion susceptibility of CRMs in such an altered metallurgical state as well as the fate of the braze material itself, especially if a braze or weld material with diminished corrosion resistance is exposed to corrosive environments. Galvanic corrosion can result when a marine environment infiltrates the core region. Hence, the possibility exists for a three-alloy (or more) macro-scale galvanic couple if the core material, face-sheet and bond region are comprised of different alloys, and/or produce solid-state compositional gradients through the bonding process. In the case of corrosion resistant materials, galvanic coupling can trigger localized intergranular, pit, or crevice-type corrosion attack depending on the alloy, heat treatment, composition and “threshold” conditions for such attack. In the case of CRMs, the primary issue in galvanic corrosion is exceeding a local corrosion “threshold” such that localized corrosion is triggered.[12] Scientifically, this identification points toward the need to identify windows of susceptibility established by threshold Cl^- ion concentration, potentials, and temperatures for each candidate CRM, braze alloy and metallurgically altered region of a CRM (due to welding and transient liquid phase bonding thermal cycle and alloying element diffusion, etc.). The corrosion resistance of super-austenitic stainless steel base materials in seawater have been determined to be adequate and cost-effective.¹ However, according to the “weakest link theory,” the single most susceptible material or phase in isolation provides the weakest link in the corrosion resistance of the structure must be considered. This includes any intermetallic or Cr-depleted phases formed in braze alloys that have low intrinsic corrosion resistance.

Moreover, the corrosion resistance of the combined face sheet/core/and bond region must be considered together in order to understand and mitigate more sophisticated corrosion modes that might degrade the properties of cellular metal structures. These include and heat treatment induced sensitization, baseplate alloying element dilution and/or melting point depressant (Si, P, B) induced degradation of the corrosion resistance of the face sheet and core materials. The potential concern associated with the braze thermal cycle induced sensitization can usually be alleviated by proper selection of low carbon, stable super-austenitic alloys with sufficient chromium content to avoid detrimental dilution.[12] A highly alloyed braze or weld metal also combats beneficial alloying element dilution. However, yet another concern is dissimilar metal crevice corrosion where an alloy with inferior corrosion resistance (e.g., the braze alloy) sandwiched with a more corrosion resistant material (e.g., Al-6XN) triggers crevice corrosion of the more resistant alloy through the local chemistry change acid-induced depassivation crevice corrosion mechanism [13]. This latter mechanism was discovered to be operative during studies in *FY 04 and 05*.

Cell type, face sheet and core materials as well as fabrication methodology and materials all might also affect the corrosion behavior of cellular metals and impact the viability of corrosion mitigation strategies. Each cellular metal geometry/concept, material and bonding method has its own set of implications with regard to corrosion resistance, and practicality of corrosion protection/mitigation strategy. Constructed metal lattices are a very affordable approach for the creation of various cellular metal structure such as tetragonal structures [14]. In one approach, Prof. Wadley's group at UVA [15] has taken expanded or perforated metal sheet containing a two-dimensional ordered array of hexagonal holes and subject them to out of plane deformation at the nodes to create a triangulated core. Transient liquid phases can then be used to bond them together in a lay up or to face sheets. Cellular structures are created by stacking the pre-crimped wire and transient liquid phase bonding the nodes [16]. However, many of the modes of

¹ Super-austenitic stainless steels are a class of highly alloyed f.c.c. non-magnetic stainless steels with excellent resistance to seawater pitting and crevice corrosion brought about through Mo and N alloying. High corrosion resistance including immunity to sensitization and stress corrosion cracking, high resistance to thermally induced formation of detrimental phases and non-magnetic properties make them ideal for marine deployment.

local corrosion discussed above that could affect commercially available braze materials in the Nicrobrazo family and a superaustenitic stainless steel such as AL-6XN are expected to be operative independent of cellular metal topographies that employ braze fabrication/bonding methods. That is because they are governed by microstructural scale processes and are independent of macroscale geometric details. Therefore, development of a single phase, high alloyed and therefore intrinsic corrosion resistant, as well as super-austenitic compatible braze will have generic (i.e., across all cellular metal topographies) benefit on the corrosion resistance of all brazed cellular structures.

Common commercially available braze alloys include silver-base filler alloys, copper-base filler alloys, nickel-base filler alloys, aluminum-base filler alloys, and iron base alloys. Nickel base braze alloys are typically used for joining stainless steels and are the most corrosion resistant for marine applications. Table 1 lists some of the commercially available braze alloys in the nickel-based class, along with their pitting resistance numbers, nominal compositions and the melting point depressants used to achieve desirable flow and melt characteristics.

Table 1. Survey of commercially available braze alloys, Nicrobrazo alloys are produced by Wall Colmonoy Corporation. AlfaNova is registered trademark of Alfa Laval and represents possibilities for future braze design. FP-613 is produced by Fukuda Corporation, and it is uncertain if it is applicable to stainless steel brazing.

Nicrobrazo Alloys	% Cr	% Ni	% Mo	% Fe	Melting point Depressant	PREN
31	22	Balance	0	0	Si, P	22
51	25	Balance	0	0	Si, P	25
110	7.9	Balance	2	0	Si, B	14.5
30	19	Balance	0	0	Si	19
3002	15	Balance	0	0	Si	15
3003	17	Balance	0	0	Si, B	17
Other Braze Alloys		Balance				
MBF-51	15	Balance	0	0	Si, B	15
FP-613	29	Balance	0	0	Si, P	29
AlfaNova	17	11	2	Balance	Si, B	23.6

The details of the potential corrosion problems encountered during brazing of cellular metal structures first requires a detailed discussion of the Nicrobrazo™ alloy metallurgy associated with the brazing process. The relative pitting and crevice corrosion resistance of cellular metal stainless steels candidate materials and Ni- or Fe-based braze alloys can be at first quantified assuming existence of a single solid solution phase with a given composition. Alloying elements chromium, molybdenum, and nitrogen in solid solution face centered cubic and body centered cubic stainless steels increase the pitting and crevice corrosion resistance of stainless steels. The beneficial effects are complex and interactive. However, the effects can be summarized as increasing the resistance to dissolution in a strong reducing acid such that the local critical crevice solution that breaks down the passive layer is not formed as readily for a variety of crevice geometries. Attempts have been made by suppliers to develop a compositionally derived pitting index, known as the "pitting resistance equivalency number" (PREN). PREN shown above in Table 1 can be determined by the compositional parameter below [12].

$$\text{PREN} = \% \text{Cr} + 3.3(\% \text{Mo}) + 16(\% \text{N})$$

Equation 1

There are some variants of PREN using factors of 3.0 for molybdenum and factors ranging from 12.8 to 30 for nitrogen [32]. For stainless steels containing tungsten, the effect is incorporated in the factor $3.3(\% \text{Mo} + 0.5\% \text{W})$ because the potency of tungsten is similar to that of molybdenum [12].

$$\text{PREN} = \% \text{Cr} + 3.3[\% \text{Mo} + 0.5(\% \text{W})] + 16(\% \text{N})$$

Equation 2

Nicrobraz 31 (Ni-21.2Cr-6.3Si-3.8P), produced by Wall Colmonoy Inc., is the braze alloy typically used in joining AL-6XN (Fe-20.5Cr-24Ni-6.3Mo-0.22N-0.02C) cellular core structures to AL-6XN face sheets. From Table 1 it can readily be seen that Nicrobraz 31 (PREN = 22) and AL-6XN stainless steel (PREN = 45.7) are not well matched to each other, nor is the PREN of Nicrobraz 31 high enough to resist corrosion in seawater.

The mis-match in PREN numbers raises concerns for three reasons: (a) the corrosion resistance of AL-6XN is good enough to enable room temperature seawater service while a material such as Braze 31 with lower PREN is not sufficiently resistant even as an ideal solid solution, (b) the difference in PREN may trigger dissimilar metal crevice attack of the more resistant AL-6XN alloy, and (c) formation of a complex ternary eutectic typical of braze alloys with only partial removal of melting point depressants results in a microstructure that is even more susceptible to corrosion than an ideal solid solution. The PREN parameter analysis if applied to individual phases based on their specific chemical compositions indicates that the microstructures formed and possible alloying element partitioning, must be taken into consideration. In ONR Grant N00014-03-1-0497 the complex multi-phase microstructure formed during brazing was characterized.

Transient liquid phase bonding requires a vacuum furnace treatment, specifically at 1150°C for 60 minutes for the system of AL-6XN and Nicrobraz 31.[17] After application of the bonding agent, the system is heated to a moderate temperature to remove the binder. It is then heated above the melting point of the transient liquid phase. Capillary forces draw much of the fluid to the nodes of the periodic cellular structure. The elements alloyed into the filler for melting temperature control, ideally, should diffuse out from the braze material into the bulk of the base metal being metallurgically bonded. Brazing conditions such as time and temperature, and brazing atmosphere needed for optimizing corrosion resistance affect the rates and extent of interdiffusion of the melting point depressants from the braze alloy to the host/base metal. Hence, the diffusion of melting point depressant elements by diffusion into the base metal ultimately governs whether a single phase Ni-Cr solution alloy can be formed. With this background in mind, a more detailed objective may be stated for ONR Grant N00014-03-1-0497.

The over arching objective of research focused on establishing and clearly identifying the corrosion mechanisms of cellular metals constructed of a super-austenitic stainless steel (Fe-24Ni-20Cr-6.3Mo-0.22N wt.%) when brazed with a commercial Nicrobraz alloy (Ni-22Cr-6.3Si-3.8P, wt.%). The following questions were addressed in this research:

- What are the windows of susceptibility of highly alloyed AL-6XN stainless steel in marine environments, and what are the windows of susceptibility of commercially available

Nicrobrazed alloys? Specifically, what are the critical chloride levels, and potentials that will cause localized corrosion to initiate and propagate in these materials when evaluated separately? Are commercially available alloys suitable for use in marine environments?

- What metallurgical factors are responsible for degrading the corrosion resistance in bonded regions of combined brazed/base alloys. Is the weakest link the braze, the heat affected zone of the base metal or in the base material when brazed joints are exposed in combination in a marine environment?
- What are the mechanisms of corrosive attack in cellular metals in marine environments? Is dissimilar metal crevice corrosion of AL-6XN possible when combined with Nicrobrazed 31 braze alloy in a crevice environment?
- What are possible mitigation strategies given the mechanisms of corrosion attack elucidated above?

TECHNICAL APPROACH

In this grant, brazed microstructures and compositions were characterized at the materials science length scale, long term corrosion exposure experiments were carried out to identify modes of attack and susceptible regions/phases in open and closed cell sandwich panels constructed of both AISI 304 stainless steel (18Cr-8Ni-0.5Mo-Fe bal) with Nicrobrazed 51 (25Cr-10P-Ni bal) and AL-6XN stainless steel (20.5Cr-24Ni-6.3Mo-Fe bal) with Nicrobrazed 31 (22Cr-6.5Si-Ni bal). Subsequent focus was directed towards AL-6XN stainless steel (Fe-24Ni-20Cr-6.3Mo-0.22N, wt. %) brazed (1150°C for 60 minutes) with Nicrobrazed 31 alloy (Ni-22Cr-6.3Si-3.8P). 304 stainless steel (Fe-8Ni-18Cr) brazed (1050°C for 60 minutes) with Nicrobrazed 51 (Ni-25Cr-10.5P) was only used as a comparison to the performance of AL-6XN structures. Diagnostic electrochemical studies were also conducted to provide a mechanistic understanding of attack modes and develop a scientific foundation for the acceptance or rejection of these materials in marine environments. The approach utilized was to study both long-term seawater exposures as well as to conduct instrumented electrochemical investigations, augmented with metallurgical analysis of braze structures in order to elucidate corrosion mechanisms. Experiments could be divided into: (a) metallurgical characterization of brazed joints, (b) studies on isolated materials including isolated thick section braze beads, (c) studies of combined materials in brazed joints of fixed dimensions, (d) studies of continuously variable brazed joints. Electrochemical tests were conducted on (a) isolated materials, (b) one sided brazed and sandwiched brazed materials consisting of a baseplate and Nicrobrazed 31 at fixed braze gap (e.g., diffusion length), and wedge shaped or variable gap brazed/base material sandwiches. The main metric for resistance was critical potentials associated with stabilization and repassivation of local corrosion and evidence of active corrosion in simulated crevice environments.

The overall approach of isolated electrochemical testing is to isolate each material/phase, as shown in Figure 1, in order to construct an overall corrosion mechanism based on the behavior of each component material. Therefore, the approach taken was:

- Dissection of cellular structures to enable investigation of the isolated regions of concern. (face-sheet, core, bonded regions, including isolated braze materials)
- Definition of critical threshold potentials for localized corrosion of both base metal, braze, and metallurgical altered microstructures.
- Compare long term open circuit potentials to threshold potentials using the criterion that $E_{OCP} \geq E_{threshold}$ identifies a condition of local corrosion susceptibility.

- Characterization of these properties over a range of NaCl concentrations typical of marine/rainwater environments. Definition of “windows of susceptibility” for local corrosion compared to expected service conditions. Prediction of results of exposure studies from electrochemical framework.
- Consider advanced forms of corrosion brought about by extrinsic alteration of properties such as wetting of grain boundaries by braze phases and dissimilar metal crevice corrosion.

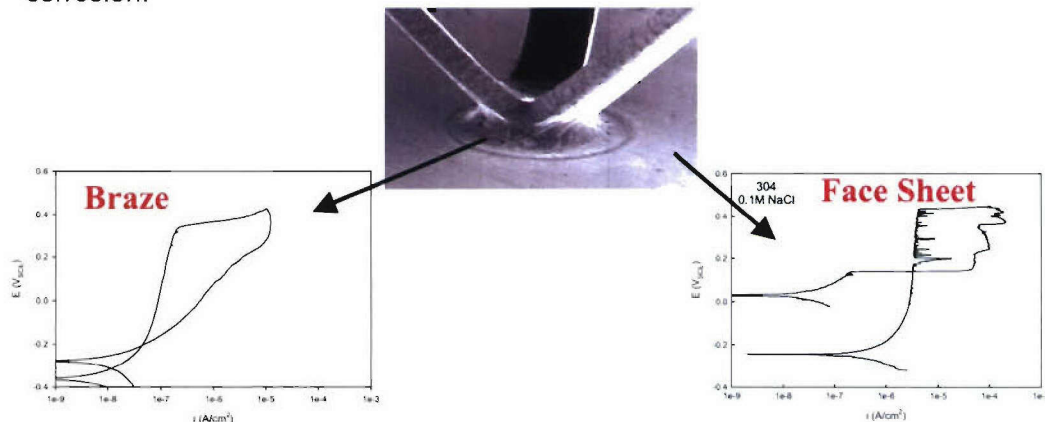


Figure 1. Investigation of isolated regions of a pyramid truss open-cell structure.
Face-sheet : AISI 304 stainless steel, polarized in 0.1M NaCl; *Braze*: Microbraz 51, polarized in 0.6M NaCl.

The overall approach of exposure testing as shown in Figures 2a and 2b was to test monolithic sheets of each stainless steel with and without braze materials as well as various sandwich panels with open and closed cells (e.g., pyramidal truss and square honeycomb). These samples were tested to determine corrosion mode (morphology) and frequency of attack of brazed sites as a function of environmental severity. Different environmental severities are considered including full immersion in 6 wt. % FeCl_3 , full immersion in ASTM Artificial Ocean Water (similar to 0.6 M NaCl) and alternate immersion in the same. The following approach was used:

- Conduct multiple crevice assembly studies on isolated monolithic materials with and without braze
- Conduct studies on closed and open cell, sandwich panels with brazed construction
- Perform post-mortem (failure analysis) consisting of metallography, scanning electron microscopy and confocal laser scanning microscopy.



Figure 2a. Sandwich truss panels-- *Top*: square honeycomb closed cell *Bottom*: pyramidal truss open cell constructed of AL-6XN stainless steel and Microbraz 31

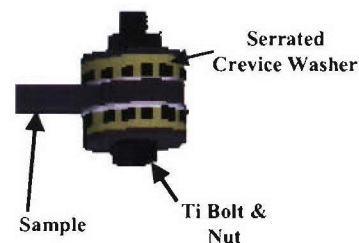


Figure 2b. Multiple crevice assembly used for crevice corrosion testing of monolithic materials indicated as sample.

The microstructure of Nicrobraz 31 on AL-6XN (1150°C for 60 minutes) was investigated using x-ray diffraction, SEM and back scattered electron imaging, as well as theoretical phase equilibrium calculations. The complex microstructure was found to be due to the presence of melting point depressants Si and P in the braze alloy, which promoted Cr₂P and Ni₃Si intermetallic phase formation during brazing thermal treatment at 1150°C. The resulting microstructure of Nicrobraz 31 on AL-6XN was found to consistently contain specific multiple phases owing to the persistent presence of P and Si melting point depressants which leads to phase equilibrium between nickel rich solid solution, Cr₂P, and Ni₃Si phases in the braze structure of two cellular metal topographies. Preferential attack of the nickel rich phases of Nicrobraz 31 was observed and rationalized to be caused by depletion of beneficial chromium.

Electrochemical methods were also used to study Al-6XN/braze joints with continuously variable joint gaps (variable diffusion length) with post-braze heat treatment. Wedge or tapered brazed samples with continually variable clearance or diffusion were brazed at 1150°C temperatures and subjected to post-braze heat treatment at 580 and 700°C. The goal of these heat treatments is to eliminate the complex ternary multi-phase by solid state diffusion of P and Si into the base alloy to form a remaining Ni-Cr solid solution in the braze. This braze might also contain Mo from the Al-6XN which would improve corrosion resistance. A tapered joint sample of variable braze gap was constructed of two bars of the base metal of AL6XN (Fe-24Ni-20.5Cr-6.3Mo-0.22N) super-austenitic stainless steel (SASS). The braze gap was filled with nickel based braze alloy, Nicrobraz 31® (Ni-22Cr-6.5Si-3.5P) and brazed for 1 hr at 1150°C. Individual potentiodynamic polarization scans carried out in 0.25 M HCl (pH=0.6). Different braze gaps were investigated and analyzed after these post-braze heat treatments in order to reveal the inverse proportionality between braze gap/diffusion length and corrosion resistance.

The period of performance was mainly dedicated to elucidating the corrosion mechanisms of a super-austenitic stainless steel Al-6XN (Fe-24Ni-20Cr-6.3Mo-0.22N) when brazed with a commercial Nicrobraz alloy (Nicrobraz 31: Ni-22Cr-6.3Si-3.8P). Investigations of subsequent Ni-Cr-Mo model alloys point to braze alloy compositions that might improve the corrosion resistance of braze alloys and enhance compatibility with AL-6XN in the context of the DMC corrosion mechanisms proposed. Alloy design was undertaken in a subsequent grant.

TECHNICAL ACTIVITIES and FINDINGS

Characterization of the metallurgy of brazed joints

Brazing conditions such as time and temperature, and brazing atmosphere needed for optimizing corrosion resistance affect the rates and extent of interdiffusion of the melting point depressants from the braze alloy to the host/base metal. Isothermal ternary phase diagram for Ni-Cr-Si system at 1125°C indicates that loss of Si via diffusion into the base metal would leave a single phase Ni-Cr solid solution. Therefore, given ample time, a braze alloy comprised of Ni-Cr-Si would result in a single phase nickel-chromium solid solution [18]. Theoretical calculations using FactStage™ phase equilibrium software to aid in identifying the phases of Nicrobraz 31 [19]. Nicrobraz 31 consists of nickel, chromium, silicon and phosphorus. The silicon and phosphorus are added in order to decrease the melting temperature of the braze alloy. Ideally, the melting point depressants diffuse away, into the bulk of the base metal material during brazing or post-braze heat treatment. For these reasons, the equilibrium phase diagrams shown below were calculated with decreasing amounts of silicon or phosphorus. Only one melting point depressant could be decreased and the other held constant to create the pseudo-

ternary phase diagrams of Figures 3-6. These equilibrium diagrams, along with x-ray diffraction patterns (not shown here) help identify the phases present in Nicrobraz 31 when brazed to Al-6XN. The nominal composition of the braze alloy is marked by the vertical red dashed line which is intersected by the horizontal red dashed line indicating brazing temperature of 1150°C. From Figure 3, which was calculated with no phosphorus present, it can be seen that 1150°C would not be high enough to melt the braze alloy. However, Figure 4 was calculated with phosphorus present (actual braze composition) and it is shown that the combination of silicon and phosphorus successfully decreases the melting temperature of the braze alloy to just below 1150°C. A similar effect is seen in Figure 5 and 6, in that the melting temperature of the alloy is higher than 1150°C if no silicon is present, but with both silicon and phosphorus the braze can be melted at this temperature. To envision the alloy location on these diagrams after the melting point depressants have diffused into the base metal and the system has cooled it can be imagined that the intersection of the red dashed lines would track diagonally to the lower left corner of the plot. From analysis of Figure 3, it is seen that as silicon is removed by diffusion into the base metal and the system is cooled below 500°C, the resulting phases are BCC chromium rich solid solution (BCC_A2), and FCC nickel rich solid solution (FCC_A1) if not completely the FCC nickel rich solid solution (FCC_A1). Similarly, from the analysis of Figure 4, it can be seen that as phosphorus is removed by diffusion into the base metal and the system is cooled below 460°C, the resulting phases are M_3P ($M = Ni/Cr$), FCC nickel rich solid solution (FCC_A1), Ni_3Si (L12_FCC), and BCC chromium rich solid solution (BCC_A2). The diffraction patterns for the suspected phases were plotted over the experimental spectra using the lines listed in the International Database of Powder Diffraction Data for isolated and identified phases. From these XRD it was concluded that FCC nickel rich solid solution certainly does exist in Nicrobraz 31 brazed at 1150°C for 60 minutes. The presence of BCC chromium rich solid solution, Ni_3P , and Ni_3Si was tentatively confirmed from XRD. From analysis of Figure 5, it would be expected that Cr_2P would exist even if all silicon and most of the phosphorus has diffused out of the Nicrobraz 31 into the base metal. Virtually, all phosphorus would have to be removed from the braze alloy in order to have single phase FCC nickel solid solution. This is indicated by the existence of the FCC nickel rich solid solution (FCC_A1) on the far left of Figure 5. The presence of the Cr_2P phase could effect the corrosion resistance of Nicrobraz 31 by tying up the chromium and therefore depleting other phases of the braze leaving it more susceptible to localized attack. Additionally, in reference to Figure 3, if phosphorus is completely removed, or never added, as the amount of silicon is reduced, any remaining Si enjoys solubility in the FCC nickel solid solution (FCC_A1), as indicated by the large phase field for FCC_A1.

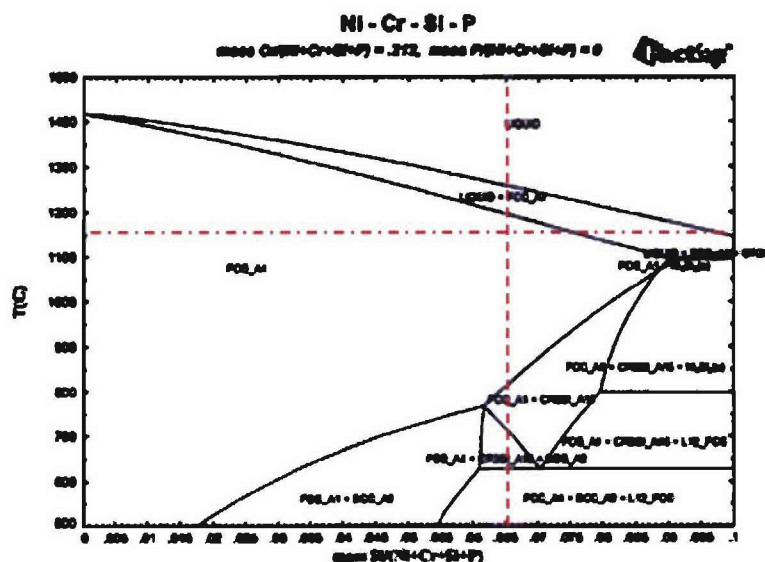


Figure 3. Calculated equilibrium phase diagram showing loss of silicon on x-axis and temperature on the y-axis. The amount of phosphorus is fixed at a value of zero. Dashed lines indicate Nicrobraz 31 composition and 1150°C brazing temperature. FCC_A1 (Ni_{ss}), BCC_A2 (Cr_{ss}), L12_FCC (Ni₃Si).

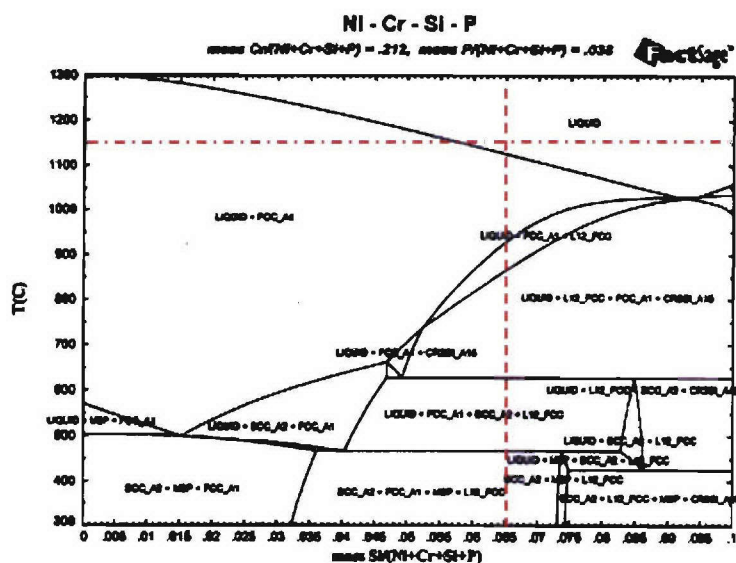


Figure 4. Calculated equilibrium phase diagram showing loss of silicon on x-axis, temperature on the y-axis. The amount of phosphorus is fixed at a ratio of $P/(\text{Ni}+\text{Cr}+\text{Si}+\text{P})=0.038$. Dashed lines indicate Nicrobraz 31 composition and 1150°C brazing temperature. FCC_A1 (Ni_{ss}), BCC_A2 (Cr_{ss}), L12_FCC (Ni₃Si), M3P (Ni₃/Cr₃Si).

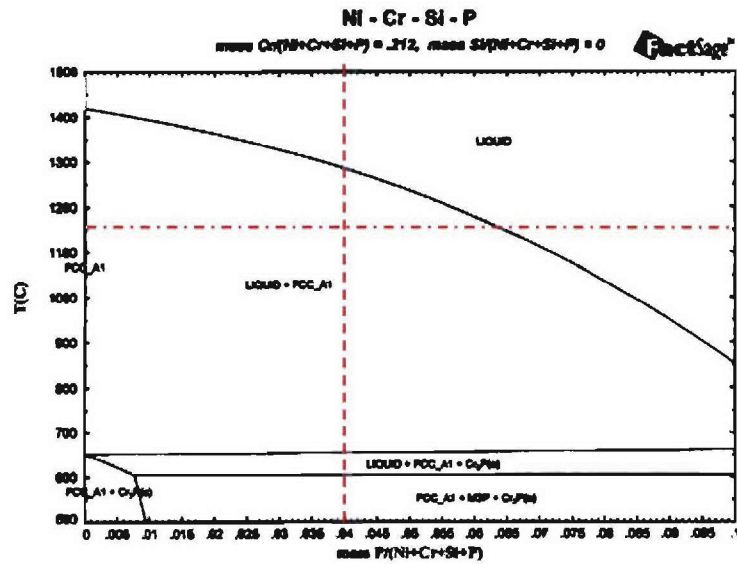


Figure 5. Calculated equilibrium phase diagram showing loss of phosphorus on the x-axis and temperature on the y-axis. The amount of silicon is fixed at a value of zero. Dashed lines indicate Microbraz 31 composition and 1150°C brazing temperature. FCC_A1 (Ni_{SS}), M3P (Ni₃/Cr₃Si), Cr₂P.

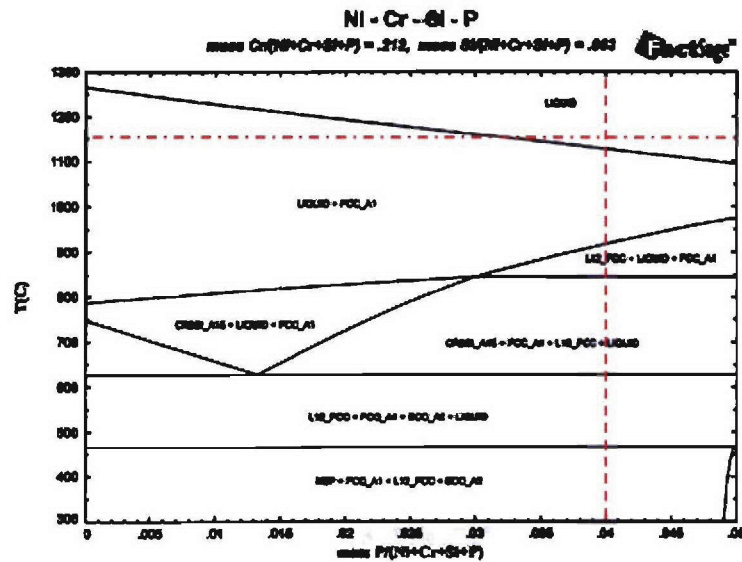


Figure 6. Calculated equilibrium phase diagram showing loss of phosphorus on the x-axis and temperature on the y-axis. The amount of silicon is fixed at a ratio of Si/(Ni+Cr+Si+P)=0.063. Dashed lines indicate Microbraz 31 composition and 1150°C brazing temperature. FCC_A1 (Ni_{SS}), M3P (Ni₃/Cr₃Si), L12_FCC (Ni₃Si).

Scanning electron backscattered and secondary electron imaging confirmed the presence of multi-phase braze microstructures suggested by phase equilibria and experimental XRD. Apparently, the melting point depressants alloyed in the braze material were not totally removed by diffusion into the base metal. For instance SEM back-scattered electron images and qualitative electron dispersion spectra collected for the above samples are shown below (Figures 7-14). In back scattered electron images, regions rich in elements with heavier atomic weights show as brighter regions, while those rich in lower atomic weight elements show as darker regions. From the below images it can be seen that Nicrobraz 31 brazed at 1150°C for 15 minutes has a very complex microstructure where elements are partitioned into certain phases. The darkest regions are rich in chromium (atomic weight, AW = 52 g/atom) while the brighter regions are rich in nickel (AW = 58.7 g/atom). Figure 7 and 9 demonstrate that the central multiphase region ("1") of the brazed joint is rich in chromium and phosphorus, compared to the region labeled "2" which is richer in iron. Figure 10 and 11 shows regions 2 and 3 with quite a lot of Fe diffused from the Al-6XN into the solid solution braze.

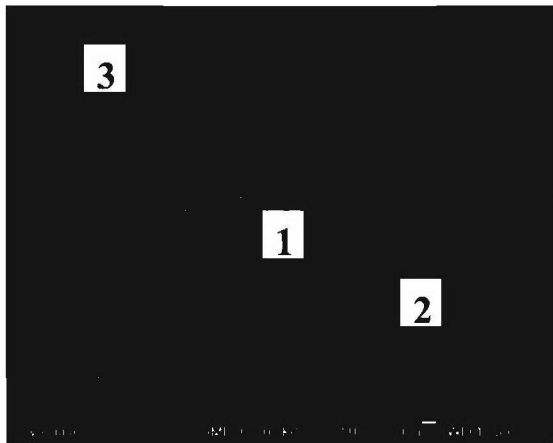


Figure 7. SEM back scattered electron image of the Nicrobraz 31/Al-6XN region in the brazed joint shown above in (1150°C/15 min.). Labels 1, 2, and 3 identify the location for EDS spot analysis shown in the figures below.

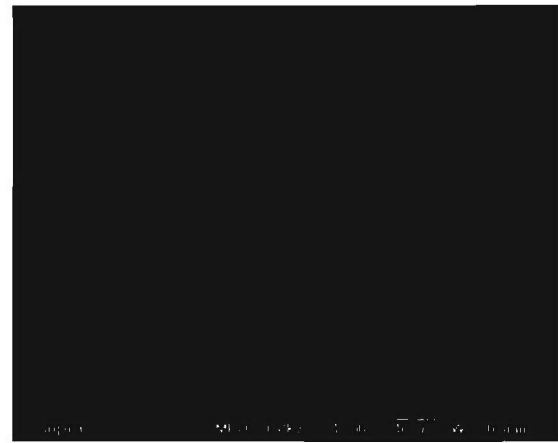


Figure 8. SEM back scattered electron image of the Nicrobraz 31/AL-6XN region in the brazed joint shown above in (1150°C/15 min.). Viewing the region labeled "1" in Figure at a higher magnification revealing the complex microstructure.

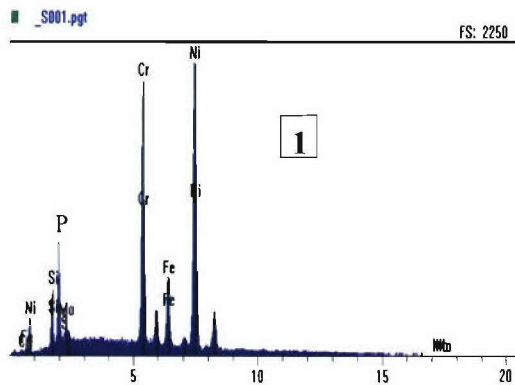


Figure 9. EDS report for the chemical composition of region "1" of the image shown in Figure .

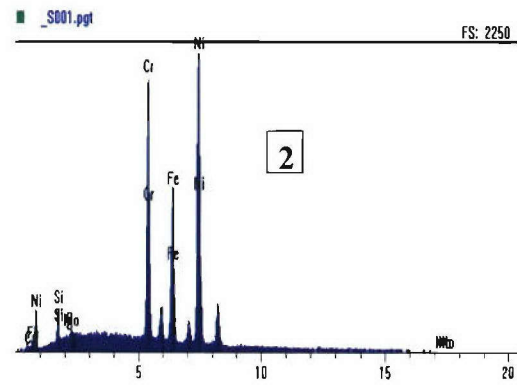


Figure 10. EDS report for the chemical composition of region "2" of the image shown in Figure .

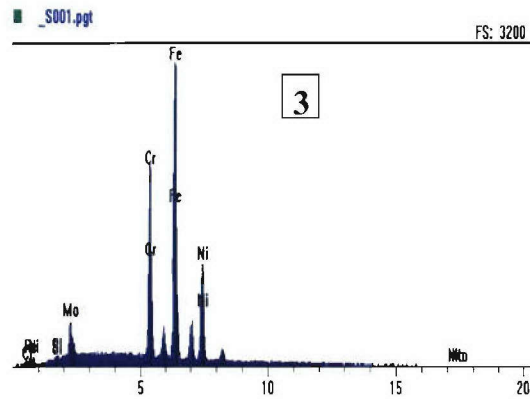


Figure 11. EDS report for the chemical composition of region "3" of the image shown in Figure .

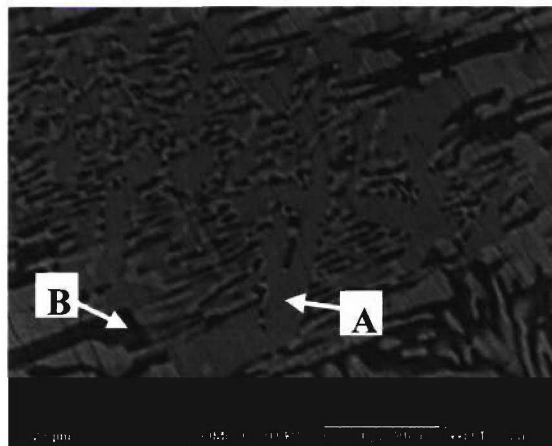


Figure 12. Higher magnification image of center region in brazed joint, brazed at 1150°C for 15 minutes. "A" and "B" markers indicate location of EDS spot analysis reported in Figure 1 and Figure 14., respectively.

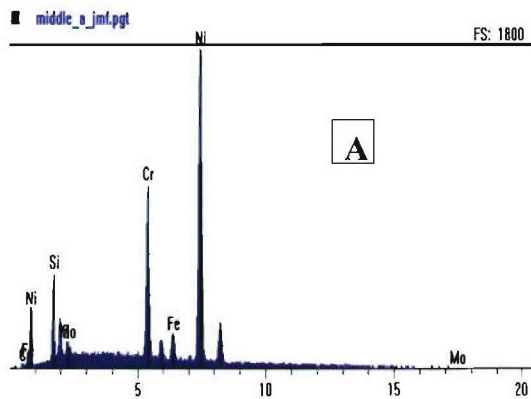


Figure 13. EDS report for the chemical composition of region "A" of the image shown in Figure .

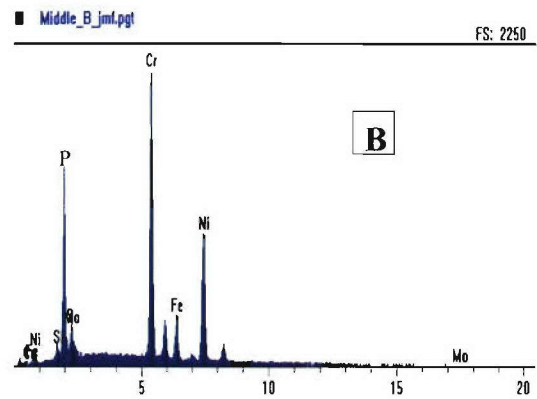


Figure 14. EDS report for the chemical composition of region "B" of the image shown in Figure .

Figure 12 show a higher magnification image of center region in brazed joint, brazed at 1150°C for 15 minutes. "A" and "B" markers indicate location of additional EDS spot analysis (Figures 13-14). The EDS spectra show that region A of the braze joint is rich in nickel and chromium deficient, where region B is rich in chromium as well as phosphorus and nickel deficient. This is consistent with the notion that the Cr_2P phase discussed, in relation to Figure 5, is present leaving the nickel solid solution chromium deficient. High resolution scanning electron microscopy in compositional mode (BSE) combined with energy dispersive X-ray spectroscopy (EDS) confirmed the presence of multi-phase braze microstructures predicted by phase

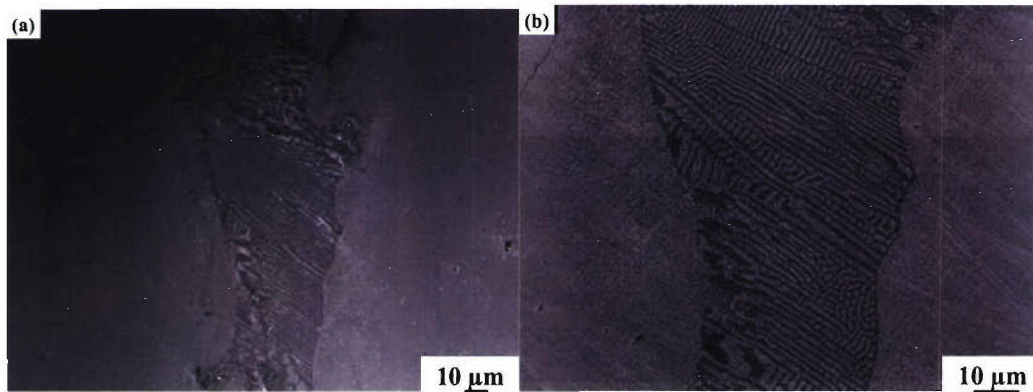


Figure 15. Low resolution secondary (a) and backscattered (b) electron images of NB31/AL-6XN (1150 °C/60 min) illustrating the width of the braze bridge region and the presence of a complex microstructure.

equilibria and experimental XRD for the native (as-received) Microbrazed 31 alloy. These results strongly suggest that the melting point depressants are not removed into the base metal. Low magnification secondary and backscattered images are shown Figure 16 (a and b) for the braze region. At low magnification, it is clear that the multi-phase structure remains following the braze treatment within a 70 μm wide region. In backscattered electron images, regions with a higher average atomic number enhance scattering and appear brighter, whereas regions with a lower average atomic number appear as darker regions. While the low resolution images above show some of these features, higher resolution imaging provides a more accurate depiction of the phases present (Figures 16a and b).

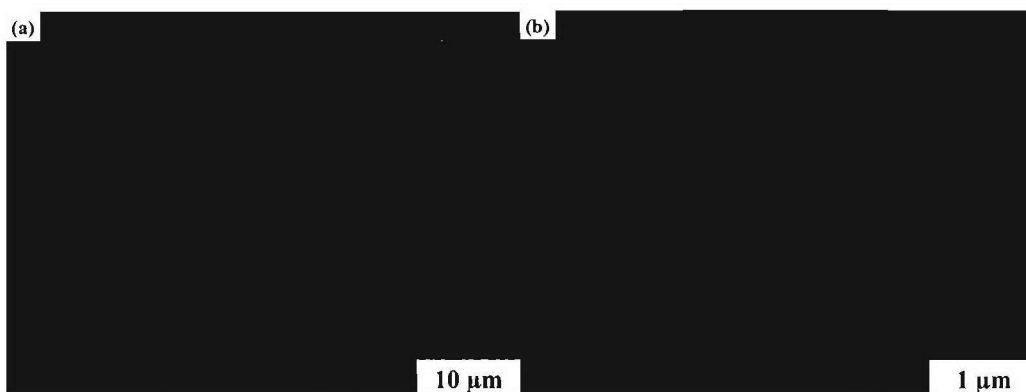


Figure 16. High resolution backscattered electron images of NB31/AL-6XN (1150 °C/60 min) showing the bridge region (a) and a higher magnification portion (b).

The higher resolution images above show that the native samples have a very complex microstructure where elements are partitioned into specific phases. Line scans were performed

to chemically analyze this behavior. The line scan (Figure 17b) was taken across two points from 1 to 2 in the image in Figure 17a. The scan data 17(b) is in direct relation to the line points labeled on the bottom of the figure. The darkest regions are rich in Cr, P and Mo while the brighter regions are rich in Ni, Fe, (AW = 58.7 g/atom) or P, Ni, and Si. This data is consistent with the previous discussions concerning the formation of Ni_xSi_y , CrP, CrMoP, and other complex phases.

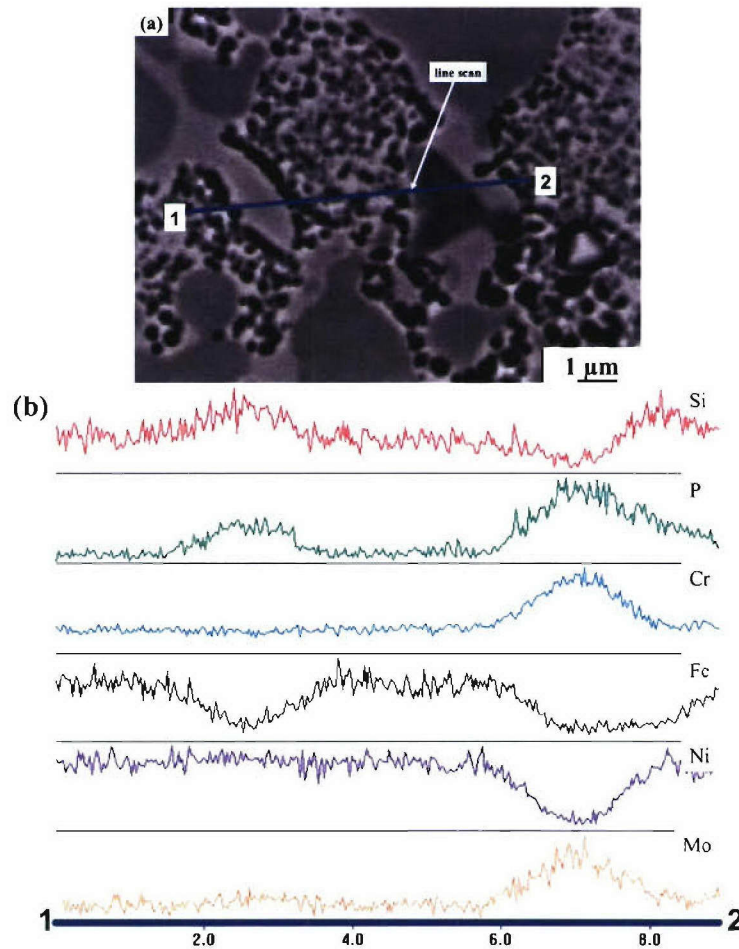


Figure 17. High resolution EDS line scan taken from the of NB31/AL-6XN (1150 °C/60 min) region along points 1, 2 in the micrograph shown in (a). The EDS line profile show clear evidence of the three phases present in the native brazed system.

Two points are clear from these studies of braze metallurgy [19]. These are that (a) the braze thermal practice used in cellular metal construction at braze clearances typically used does not result in complete diffusion of melting point depressants from Nichrome 31 into the base metal, and (b) the complex multi-phase microstructure results in Cr partitioning and likely reduced corrosion resistance as is abundantly clear from Equations 1 and 2. In subsequent studies it was found that Cr depleted regions were the most susceptible to corrosion and that corrosion initiated at these phase in the braze alloys and propagated into the Al-6XN superautenitic stainless steel alloy. Corrosion research studies under *ONR N00014-03-1-0497* confirmed these suspicions.

Long Term Corrosion Exposure Experiments on Combined and Isolated Materials

Long term exposure studies were completed to identify modes of attack and susceptible regions/phases in open and closed cell sandwich panels constructed of AISI 304 stainless steel with Nicrobraz 51 and AL-6XN stainless steel with Nicrobraz 31. Studies were conducted on both isolated and combined materials. Sites were counted if staining or crevice attack was observed.

Figure 18 a and b shows a summary of the analyzed multiple crevice assembly sites results where crevice corrosion initiated for each alloy type, or system in ferric chloride and synthetic seawater. The number of sites initiated is an indication of corrosion susceptibility. AL-6XN was found to be intrinsically resistant to pitting and crevice corrosion in marine environments at room temperature, as indicated by its performance in multiple crevice assembly exposures and electrochemical examinations. For instance, in 6 wt% FeCl_3 , isolated AL-6XN was attacked at 7% of the crevice sites applied. The alloy was not attacked at any crevice sites in full immersion in synthetic seawater. In alternate immersion in synthetic seawater, crevice corrosion was initiated at only 2.8% of the crevice sites created. The attack of other austenitic stainless steel alloys, such as 304, 316L, and 317LN was much more substantial in these environments. This intrinsic resistance was related to a high PREN number for AL-6XN due to its high content of molybdenum and nitrogen. These results are consistent with existing literature on these alloys.

It can be seen that bare AL-6XN (red) suffers little crevice corrosion while AL-6XN brazed with Nicrobraz 31 (orange) suffers from greater crevice attack in all three environments. Brazing AL-6XN with Nicrobraz 31 ($1150^\circ\text{C}/60$ minutes) produced an extrinsic mode of crevice corrosion. From multiple crevice assembly tests in 6wt% FeCl_3 , the brazed alloy was attacked heavily on the brazed surface and not at all on the bare AL-6XN surface (Figure 19). The crevice corrosion attack greatly exceeded the thickness of the Nicrobraz 31 layer, indicating that AL-6XN had also been attacked. Through visual inspection of the specimen, it was observed that attack proceeded into the AL-6XN base metal via grain boundaries (Figure 20). These observations were duplicated after electrochemical experiments in the less aggressive solution of 0.6 M NaCl with neutral pH and minimal electrochemical polarization (0 to +100 mV_{SCE}). Specifically, at 0 mV SCE, it was observed that the depth of attack was roughly 100 μm . This attack developed in 24 hours, indicating a rate of 100 $\mu\text{m}/\text{day}$.

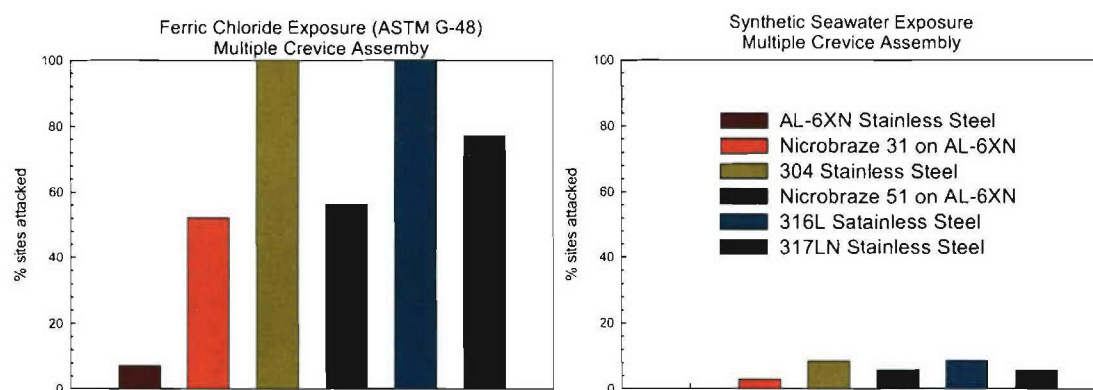


Figure 18. A summary of the results obtained in (a) ferric chloride and (b) full immersion in synthetic seawater. The figure shows the percentage of sites that were attacked. AL-6XN was not attacked in seawater. Sites were counted where staining was observed. Brazing of NB31 and NB 51 on AL-6XN ($1150^\circ\text{C}/60$ min)

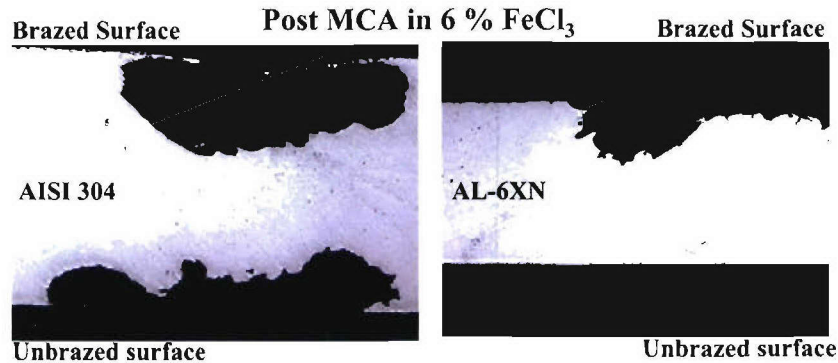


Figure 19. Micrograph of corroded multiple crevice assembly. *Left:* 304 top surface brazed (Microbrazed 51 1050°C/60 min); *Right:* AL-6XN top surface brazed (Microbrazed 31/1150°C/60 min). Samples were exposed in multiple crevice assembly to Ferric chloride for 48 hours (ASTM G-48)

Hence, the AL-6XN/Microbrazed 31 combination produced a unique extrinsic mechanism for attack of AL-6XN that is triggered by exposure to corroding Microbrazed 31 (Figure 19) in the severe 6% FeCl₃ solution. In contrast, Braze 51 on AISI 304 stainless produces an entirely different result (Figure 19) explained by the fact that this particular braze composition is more corrosion resistant than the 304 stainless steel substrate. Here, the braze is resistant to attack while pinholes exposing the 304 leads to corrosion of the underlying alloy.

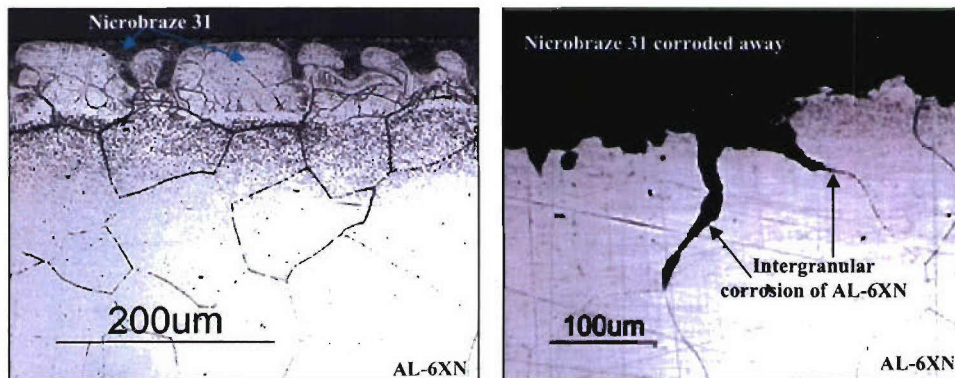


Figure 20. Micrograph of corroded multiple crevice assembly. *Left:* Microbrazed 31 (1150°C/60 min) on AL-6XN etched with etchant 88 (ASTM E-407); *Right:* Post MCA FeCl₃ exposure (ASTM G-48)

The mechanisms of corrosion attack of brazed AL-6XN base material also studied. Three mechanisms are proposed to explain corrosion of the otherwise resistant AL-6XN when brazed; these are (1) intergranular corrosion by intrinsic sensitization of AL-6XN by the thermal cycle, (2) intergranular corrosion by extrinsic sensitization of AL-6XN explained by braze penetration along the stainless steel grain boundaries as seen in Figure 20 and (3) dissimilar metal crevice corrosion (DMCc), where Microbrazed 31 crevice corrosion induces initiation of crevice attack in AL-6XN, or (3) a combination of these two modes of attack which can be seen in Figures 5. This attack of Microbrazed 31 and AL-6XN was attributed to the combination of extrinsic sensitization caused by wetting of the braze alloy along the grain boundaries of the super-austenitic stainless

steel and dissimilar metal crevice corrosion (DMCc). Intrinsic sensitization based on the braze thermal cycle was ruled out based on intergranular corrosion testing of unbrazed SASS after braze thermal treatment. Sensitization was not observed owing to the low carbon content of AL-6XN. Dissimilar metal crevice corrosion was due to easy depassivation and corrosion of Nicrobraz 31. The depassivation and lack of intrinsic crevice corrosion resistance of Nicrobraz 31 led to the development of a saturated nickel chloride solution, with low pH and high chloride content, in the occluded crevice environment. By electrochemical investigations, this harsh solution formed by initial corrosion of the Nicrobraz 31 alloy was found to depassivate and actively corrode AL-6XN. The path of corrosion along the grain boundaries of AL-6XN was found to be due to Nicrobraz 31 penetration by wetting and solidification along the AL-6XN grain boundaries followed by dissimilar metal crevice corrosion.

The structural ramifications are that joints may corrode at sites where the braze is present when the braze material possesses inferior corrosion properties in marine environments and that corrosion may propagate into the base sandwich material. This mode of attack could compromise structural integrity of sandwich structures exposed in marine environments. If a cellular panel is constructed with AL-6XN face sheets of about 2,500 μm thickness brazed with Nicrobraz 31, the structure could be completely penetrated in 25 days. Furthermore, a potential of only 0 mV SCE is very reasonable for stainless steel structures in marine environments. Crevice corrosion exposures demonstrated superior performance of isolated AL-6XN and degraded performance of AL-6XN when brazed with Nicrobraz 31 attributed to the difference in pitting resistance equivalency numbers of the AL-6XN compared to Nicrobraz 31. It is expected that if the PREN of the braze alloy could be raised to meet or exceed that of the AL-6XN this severe crevice corrosion would not be observed.

The results listed above concerning the mechanistic aspects of Nicrobraz 31/AL-6XN corrosion would be applicable to any cellular metal topology, or design constructed of these materials. This is because similar gaps (diffusion lengths) would be expected to result in the same braze microstructure and dissimilar metal crevice corrosion in AL-6XN regardless of topology and macroscopic geometry. It cannot be stated that any particular sandwich structure and associated braze geometry would be better than another from this perspective for corrosion resistance, and the bottom line is that structures made of AL-6XN brazed with Nicrobraz 31 do not offer corrosion characteristics required for the proposed applications of cellular metals.

Electrochemical Diagnostic Studies to Elucidate Mechanistic Information on Isolated and Combined Facesheet/Core alloys and Braze Materials

Diagnostic electrochemical studies were also conducted in FY 05 to provide a mechanistic understanding of attack modes, develop an understanding of windows of susceptibility and shed light on the mechanisms of corrosion that govern susceptibility. In terms of understanding windows of susceptibility, the criterion for susceptibility is that the open circuit potential of the material equals a critical potential associated with the onset of localized corrosion (e.g., $E_{ocp} \geq E_{crit}$).

Isolated Materials

A summary of critical pitting/crevice corrosion initiation and repassivation potentials for the isolated Nicrobraz 31 bead electrode is shown in Figure 21a. Below the dashed blue line (crevice repassivation), no localized corrosion of the braze 31 in isolation is expected to occur. Above the solid black line (pitting initiation), pitting and crevice corrosion would be expected. The open circuit potential measured for Nicrobraz 31 (orange box) is just above or roughly equal to the lower limit for crevice corrosion in 0.6 M NaCl, shown in Figure 21a. Galvanic corrosion in contact with AL-6XN exacerbates this problem. From this analysis it can be expected that thick sections of Nicrobraz 31 would be susceptible to crevice corrosion in seawater. Further summarizing the data for isolated cellular metal construction materials, Figure 21b shows the crevice corrosion repassivation potentials for several alloys as a function of chloride concentration. This crevice corrosion repassivation potential is the lower limit of a window of susceptibility for each alloy in neutral chloride containing environments. The result clearly demonstrates that AL-6XN is far more superior to the rest of the alloys and that Braze 31 represents the “weak link” in brazed sandwich construction using AL-6XN SASS.

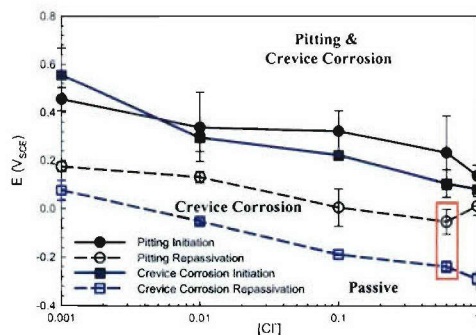


Figure 21a. Summary of critical potentials for local corrosion on multi-phase Nicrobraz 31 beaded electrodes. All solutions were deaerated, with neutral pH, at ambient temperature. The orange box indicates open circuit potential range in seawater.

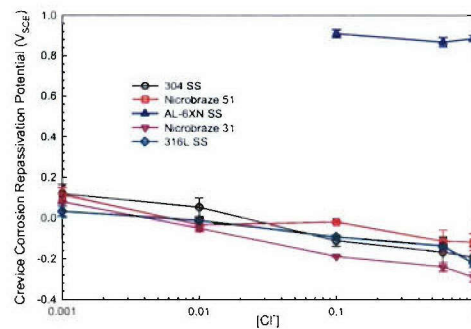


Figure 21b. Summary of crevice repassivation data presented for isolated materials. AL-6XN is far more resistant than all the other alloys, and is completely resistant to crevice corrosion at lower concentrations of Cl^- at ambient temperatures.

Combined Materials

Tests were also conducted on the brazed AL-6XN in combination with Nicrobraz 31, and the resulting corrosion resistance of the alloy system as combined materials. A flat sheet was brazed on one side and sandwiched in a crevice assembly. Figure 22 shows a comparison of brazed AL-6XN (combined) and unbrazed, isolated AL-6XN in an E-log(i) plot when creviced. There is a huge decrease in crevice corrosion resistance, expressed as critical crevice corrosion initiation and repassivation potential, once AL-6XN is brazed. This was a suspected result considering the large difference in local corrosion resistance of the two alloys and results from dissimilar metal crevice corrosion (DMCc). A summary of critical crevice corrosion initiation and repassivation potentials for AL-6XN stainless steel brazed with Nicrobraz 31 is shown in Figure 23.

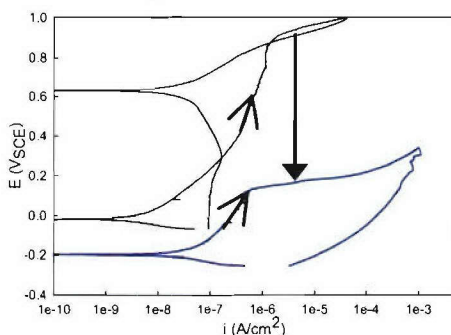


Figure 22. Comparison of crevice corrosion resistance of AL-6XN (black) and AL-6XN brazed with Nicrobraz 31 (blue -1150°C/60 min). Both scans conducted in 0.6 M NaCl at room temperature, with crevice assembly torqued to 75 in.-lbs.

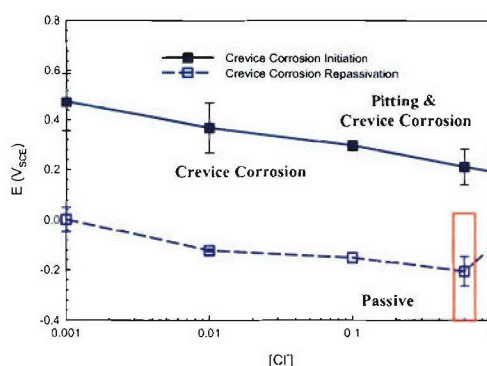


Figure 23. Summary of critical potentials for crevice corrosion for AL-6XN stainless steel flag electrodes brazed with Nicrobraz 31 (1150°C/60 min). All solutions deaerated, neutral pH, and at ambient temperature. Orange box indicates open circuit potential range in seawater

At combinations of potential and chloride concentration below the dashed blue line (crevice repassivation potential), no localized corrosion is expected to occur. Above the dotted blue line (crevice corrosion initiation) crevice corrosion would be expected when AL-6XN is brazed with Nicrobraz alloy 31. The open circuit potential measured for the AL-6XN/Nicrobraz 31 system in Figure 16 is well above the lower limit for crevice corrosion at 0.6 M chloride concentration (crevice repassivation potential). From this analysis it can be expected that the AL-6XN/Nicrobraz 31 system would be susceptible to crevice corrosion in seawater at 25°C. Comparison of Figures 21 and 23 indicates that the corrosion resistance of AL-6XN is degraded by joining with Braze 31 alloy. The mechanism for this degradation could be sensitization of AL-6XN such as by chromium phosphide formation, dilution of alloying elements lost from the base material, and dissimilar metal crevice corrosion (DMCc). Studies of DMCc (not shown) were conducted in FY 05 to confirm or refute this mechanism. Results to date support this mechanism. In short, corrosion of braze 31 triggers formation of an acidified solution that attacks AL-6XN.

Another related aspect concerning these studies of combined materials in brazed joints is the issue of sensitization of AL-6XN either intrinsically due to the thermal cycle in brazing or extrinsically due to phosphorus entry from the braze and subsequent chromium phosphide formation. The former can be dismissed based on studies of sensitization of isolated AL-6XN following a simulated braze cycle which revealed no sensitization.

In efforts to completely understand the Microbrazed 31 microstructure and its role in corrosion resistance, different braze alloy geometries have been considered. First the multi-phase beaded Microbrazed 31 electrode represented the worst case scenario in that there was no base metal “sink” for the melting point depressants to diffuse into, meaning that maximum partitioning and segregation of melting point depressants and associated detrimental phases was seen. Second was the above sandwich geometry with Microbrazed 31 brazed onto AL-6XN sheet at a narrow gap (100 μm) which could represent the best case scenario in that the melting point depressants can diffuse into AL-6XN and a thin braze layer is formed. This is the configuration that was investigated in the SEM/EDS study. An image of this sample, brazed at 1150°C for 60 minutes, tested for crevice corrosion in 0.6 M NaCl is shown below in Figure 24. The same observations that were made in the first two braze geometries discussed are seen below in the brazed joint. The solid solution nickel phases and the fine nickel rich phases are preferentially attacked. A comparison of the E-i polarization experiments for the three braze geometries is shown below in Figure 25. It can be seen that even with a narrow joint and small diffusion length $\sim 100 \mu\text{m}$, that DMCC has still occurred as evidenced by the deep attack in the braze alloy propagating into the AL-6XN stainless steel.

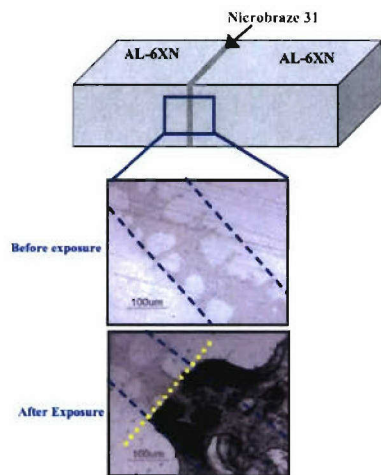


Figure 24. Configuration for AL-6XN joined with Microbrazed 31, brazed at 1150°C for 60 minutes. Yellow line marks the edge of the crevice former that was tightened to a torque of 45 in-lbs. The solution was deaerated 0.6 M NaCl at neutral pH. The exposure consisted of 1 hour at open circuit and an anodic polarization scan

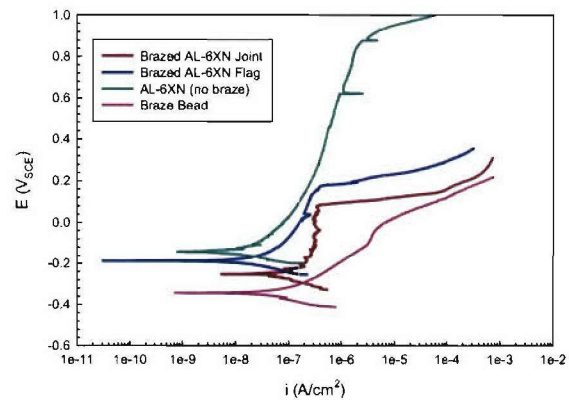


Figure 25. Comparison of anodic polarization scans for different Microbrazed 31 geometries on AL-6XN (1150°C/60 min) in comparison to isolated braze and AL-6XN materials. All scans were conducted in deaerated 0.6 M NaCl at neutral pH. Crevice tightness varied in that the flag electrode assemblies had a torque of 75 in-lbs, the brazed joint assembly torque was 45 in-lbs, and the bead assembly was <75 in-lbs.

The next stage of this work was to examine smaller diffusion lengths and longer braze times. High brazing temperatures, long brazing times, post-braze heat treatments and short diffusion lengths all promote formation of optimal single phase solid solution microstructures that offer the best possibility of high corrosion resistance and mitigation of dissimilar metal corrosion. For example, AL-6XN stainless steel butt joints were made using Microbraz 31 in a series of brazing temperatures and times at brazing temperature. Figures 26 a and b show optical images of joints brazed at 1150°C for 15 minutes and 60 minutes, respectfully. The figures show that the braze solid solution phase is more abundant when more time is allowed at the brazing temperature. The isothermal ternary phase diagram for Ni-Cr-Si rationalizes this observation.

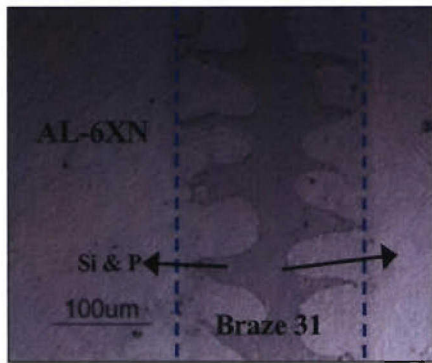


Figure 26a. Optical micrograph of AL-6XN joint brazed with Microbraz 31 (inside blue lines). Brazing conditions were 1150°C for 15 minutes in a vacuum furnace. Arrows indicate diffusion of melting point depressants, silicon and phosphorus into the AL-6XN base metal.

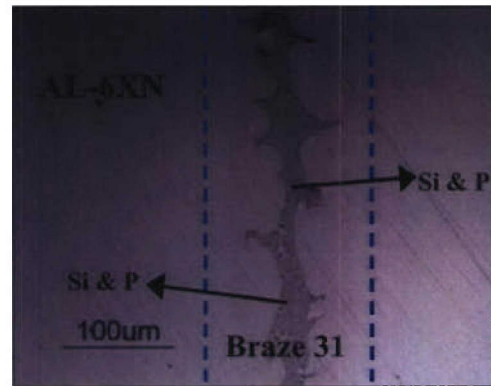


Figure 26b. Optical micrograph of AL-6XN joint brazed with Microbraz 31 (inside blue lines). Brazing conditions were 1150°C for 60 minutes in a vacuum furnace. Arrows indicate diffusion of melting point depressants, silicon and phosphorus in the AL-6XN base metal.

ELUCIDATION OF TIME-TEMPERATURE-DIFFUSION LENGTH COMBINATIONS DURING BRAZING THAT PROMOTE FORMATION OF SINGLE PHASE BRAZE MICROSTRUCTURES

A similar effect can be produced by reducing the diffusion length (gap or clearance) at a fixed temperature and diffusion time. A wedge shape or continually variable brazed joint was investigated as a novel way to continuously vary diffusion length (Figures 27-29). This wedge shaped joint was made with AL-6XN on both sides with Microbraz 31 in the middle. A wedge shaped sample provides a continuously variable crevice gap that enables the determination of the diffusion length needed to achieve a single phase solid solution alloy. In theory, a short diffusion distances in combination with longer diffusion times and higher temperatures should promote formation of a single phase microstructure. Preliminary experiments conducted at various braze times and temperatures on Microbraz 31 brazed on AL-6XN were conducted to confirm the possibility of improved corrosion resistance. For example, a single phase braze alloy would be expected to have greater corrosion resistance than a multi-phase material, due to the uniformity of beneficial alloying elements and a lack of Cr partitioning. Figures 27 and 28 taken

from the cross-section of a continuously brazed joint indicate that the most narrow brazed joint does have improved corrosion resistance (because it approaches a single phase fcc Ni-Cr microstructure) but also shows that it is still more susceptible to corrosion than AL-6XN.

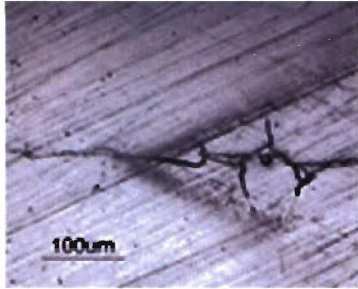


Figure 27. Corrosion of wedge sample (NB31/AL-6XN (1150 °C/60 min) shown in Figure 29. Corrosion site was 1 cm right of the end set at 0 clearance. Site was exposed in deaerated, neutral 1.0M NaCl and polarized to 1V_{SCE}.

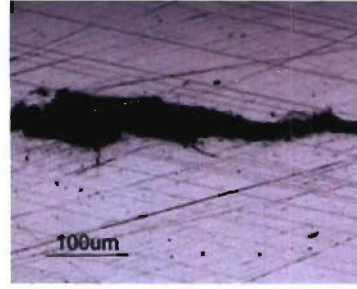


Figure 28. Corrosion of wedge sample (NB31/AL-6XN (1150 °C/60 min) shown in Figure 29. Corrosion site was 3 cm right of the end set at 0 clearance. Site was exposed in deaerated, neutral 1.0M NaCl and polarized to 1V_{SCE}.

ELUCIDATION OF POST-BRAZE HEAT TREATMENT TIME-TEMPERATURE-DIFFUSION LENGTH COMBINATIONS THAT PROMOTE FORMATION OF SINGLE PHASE BRAZE MICROSTRUCTURES

In FY 06 we began to explore thermal cycle and braze heat treatments-diffusion distance combinations that optimize melting point depressant diffusion into the base metal in order to promote formation of a single face braze microstructures the most optimal for corrosion resistance in brazed cellular metal joints exposed in marine environments. This work will be continued in FY 06 and in a subsequent ONR grant. Wedge or tapered brazed samples with continually variable clearance or diffusion were brazed at 1150°C temperatures and subjected to post-braze heat treatment at 580 and 700°C. The goal of these heat treatments is to eliminate the complex ternary multi-phase and form a single phase Ni-Cr solid solution perhaps containing Mo from the Al-6XN for improved corrosion resistance.

A tapered joint sample of variable braze gap was constructed of two bars of the base metal of AL6XN (Fe-24Ni-20.5Cr-6.3Mo-.22N) super-austenitic stainless steel (SASS) as shown in Figure 29a. The braze gap was filled with nickel based braze alloy, Nicrobraz 31© (Ni-22Cr-6.5Si-3.5P) and brazed for 1 hr at 1150°C (Figure 22b). To reiterate the findings to date, upon brazing Nicrobraz© 31 (Ni-22Cr-6.5Si-3.5P) to AL-6XN (SASS), a multi-phase microstructure forms. At narrow gaps a near solid solution of Ni-Cr forms, but as braze clearance becomes wider the multi-phase microstructure is present in the braze region. Additional corrosion tests were conducted at selected positions of this variable gap wedge to determine the effect of diffusion length and time on the corrosion resistance of brazed SASS cellular metal panels. Individual potentiodynamic polarization scans carried out in 0.25M HCl (pH=0.6) representing different braze gaps were conducted as shown in Figure 29b and analyzed to reveal the inverse proportionality between braze gap/diffusion length and corrosion resistance. A wider braze clearance correlates with a poorer corrosion resistance as evident from Figure 29 (b). The isolated braze material exhibits an active passive transition and pits just after passivation near +0.1 V SCE. At position number 3, the brazed sample pits readily at its open circuit potential.

However, at position 1, the brazed sample is substantially improved (e.g., it is passive and displays a high pitting potential).

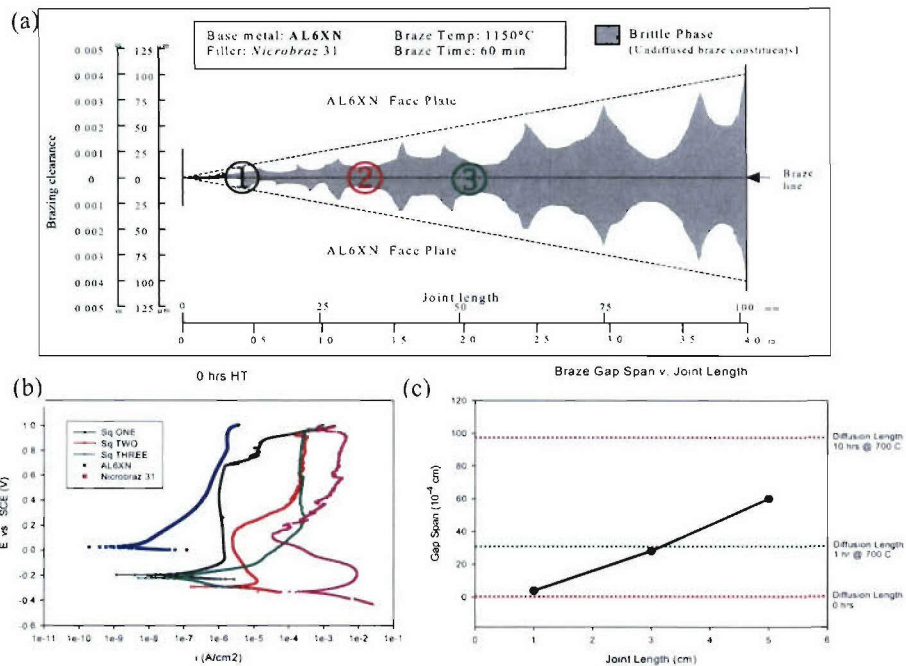


Figure 29. (a) Schematic of braze microstructure (Microbraz 31) as a function of braze clearance between regions of base metal, AL6XN SASS. (b) Potting behavior as a function of braze gap at 0 hrs HT (1150 C / 1 hr brazing process) compared to isolated AL6XN(blue) and Microbraz 31(light purple); all in deaerated 0.25M HCl. (c) Braze gap span vs. tapered joint length with diffusion length at 700 C highlighted for 0, 1 and 10 hrs HT.

Scanning Electron Microscopy (SEM) was utilized in conjunction with Energy Dispersive Spectroscopy (EDS) to determine the elemental distribution within the complicated undiffused microstructure across the braze region (Figure 30). Secondary electron imaging also shows that the multi-phase undiffused braze microstructure becomes more complicated as the braze gap, and thus diffusion length, grows larger. The provided EDS line scans show that necessary melting point depressing elements such as silicon and phosphorus are not fully dispersing by solid state diffusion into solid solution of the SASS, but instead remain largely within the braze microstructure in the form of brittle phase phosphides and silicides during the brazing process. Phosphorus, particularly, which is very proficient at depressing the filler alloy melting point exhibits little to no dissolution into the base metal. Another notable deduction from the EDS elemental line scans is the presence of molybdenum, though partial into the braze region, which originates from the host metal, AL6XN. Moreover, the chromium content becomes slightly inhomogenous in the center of the brazed region at the wider braze clearances. This suggests that during the brazing process, valuable corrosion resisting elements, such as chromium are being depleted from the Ni-Cr solid solution as a result of brittle Cr-P phase phase formation by the melting point depressants which are insoluble into Ni-Cr solid solution. As the braze clearance is reduced, the frequency of brittle phase formation diminishes and an improved corrosion resistance is witnessed.

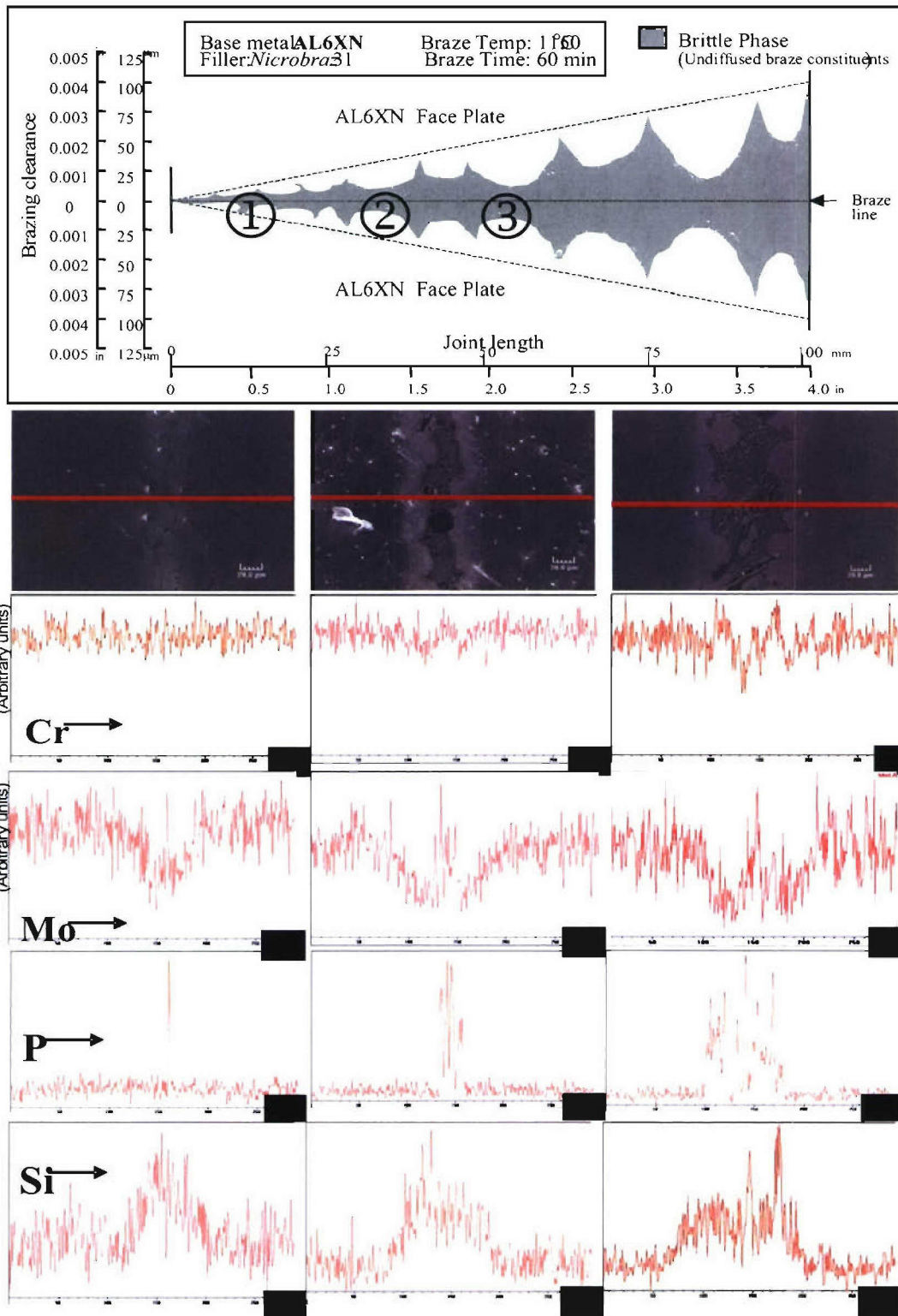


Figure 30. EDS line scans across the undiffused braze region (300 micron span) detail the elemental distribution (Cr, Mo, P, Si) of selected braze gap spans; 0 hrs of HT (1 hr at 1150 C brazing process)

Heat treatment serves as an approach to alleviate the problem associated with brittle phase formation and their effect on the system's corrosion resistance. Figure 29c indicates the interstitial diffusion distance as a function of heat treatment time. Using the theory of solid state diffusion kinetics (Figure 29c) it can be seen that very short diffusion times at 700 C will promote solid state diffusion of P over the distances necessary to homogenize the braze structure

Three samples of varying braze gap/ diffusion length have been characterized for microstructural trends and electrochemical corrosion behavior at each distinct stage of a designed heat treatment sequence. The characterization sequence used consists of analysis at 0 hrs (1 hr at 1150°C brazing process), 1hr of post-braze heat treatment under vacuum at 700°C and 10hrs of post-braze heat treatment under vacuum at 700°C. Figure 29c indicates possible diffusion distances. After each heat treatment the three samples were imaged using Scanning Electron Microscopy (SEM) and scanned for elemental distribution across the braze region via Energy Dispersive Spectroscopy (EDS). The secondary electron images and EDS line scans did not discern large change in microstructure at any stage of the sequence (these are not shown). However, electrochemical analysis displayed a marked improvement in corrosion resistance after each heat treatment.

Displayed in the E-log(i) pitting scan plots shown in Figure 30 the sample taken from the narrowest braze gap (1) exhibited an increase in pitting potential comparable to the highly corrosion resistant base metal, AL6XN super-austenitic stainless steel, even after the first hour of heat treatment. Also, via interpretation of the fully reversed polarization curve, it did not pit at all within the limits of the potentiodynamic scan after the 10 hr heat treatment stage. Subsequently, the samples from locations for the other braze gaps/diffusion lengths exhibited monotonically increased corrosion resistance with heat treatment time. However, none of these remained unpitted in the deaerated, 0.25M HCl solution over the duration of the scan. Moreover, an active/passive transition was observed in isolated braze beads indicative of Cr depletion which can be suppressed by post-braze heat treatment for even 1 hr at positions 1 and 2 that represent narrow gaps and this shorter diffusion lengths.

Electrochemical behavior with respect to braze gap clearance after post-braze heat treatment is further evidenced by a plotting of pitting potentials and repassivation potentials at each heat treatment stage (Figure 31). Pitting and repassivation potentials are increased by post-braze heat treatment time. The braze microstructures approaching a single phase Ni-Cr solid solution is far more corrosion resistant than complex multiphase microstructures shown above. Moreover, the braze microstructure can be manipulated by braze time-temperature or post-braze heat treatment. Preliminary results confirm this hypothesis as shown in Figure 31 and summarized in Figure 32. An interesting issue is the improvement brought about at position number 1 at narrow braze gap which is attributed to the solid solution formed but also results from Mo diffusion from the SASS baseplate. Improved corrosion resistance is observed. The braze microstructures approaching a single phase Ni-Cr solid solution with the addition of Mo is far more corrosion resistant than complex multiphase microstructures shown above. However, the gain of Mo in the braze structure results in depletion from the base material SASS. Such depletion could be avoided by adding Mo to the braze alloy as is done in the case of weld filler metal recommended for SASS.

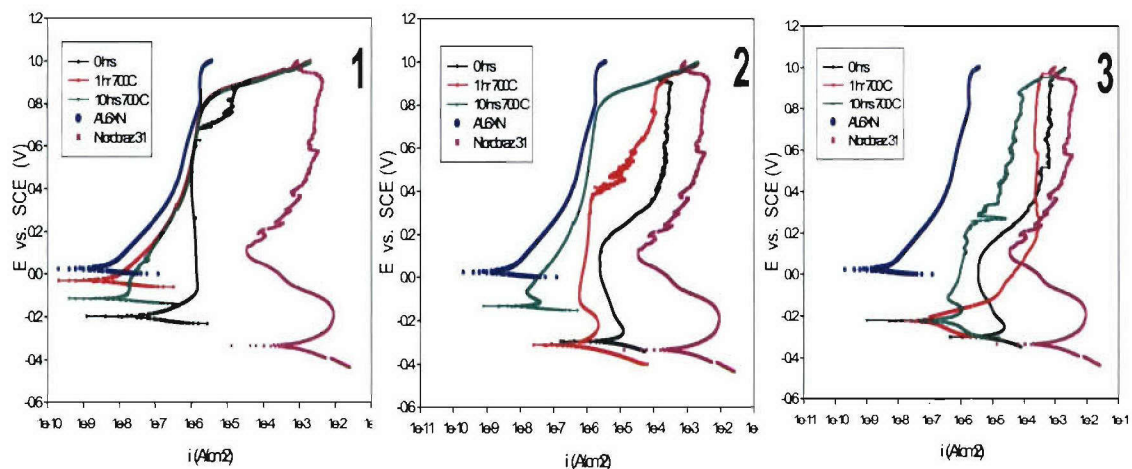


Figure 31. Electrochemical results in deaerated, 0.25M HCl, uncreviced and with respect to the indicated HT time and temperature at each position. (1)= smallest gap, (2) intermediate, and (3) widest gap clearance. E-log(i) data shown in blue and light purple are for isolated base metal and braze bead, respectively. Braze conditions were 1150°C for 60 minutes for Nicrobarze 31 brazed to Al-6XN followed by post-braze heat treatments at 0, 1 or 10h at 700 C.

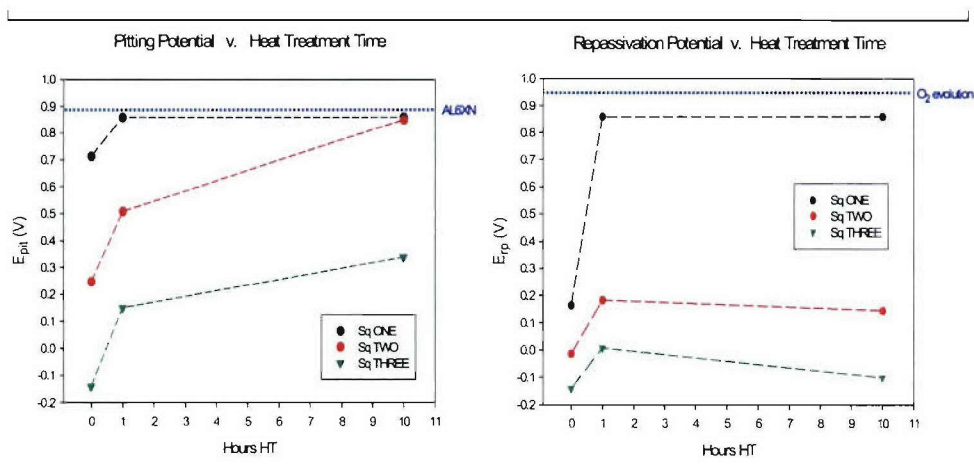


Figure 32. Summary of (a) pitting potentials and (b) repassivation potentials with respect to post-braze heat treatment time for each of the three distinct braze gap/diffusion length positions. Braze conditions were 1150°C for 60 minutes followed by post-braze heat treatments at 0, 1 or 10h at 700 C..

SUMMARY OF TECHNICAL FINDINGS

In summary, the following conclusions were reached from this research:

1. AL-6XN base material was found to be intrinsically resistant to pitting and crevice corrosion in marine environments at room temperature, as indicated by its performance in multiple crevice assembly exposures and electrochemical examinations. For instance, in 6 wt% FeCl_3 , AL-6XN was attacked at 7% of the crevice sites applied. The alloy was not attacked at any crevice sites in full immersion in synthetic seawater. In alternate immersion in synthetic seawater, crevice corrosion was initiated at only 2.8% of the crevice sites created. The attack of other austenitic stainless steel alloys, such as 304, 316L, and 317LN was much more substantial in these environments. This intrinsic resistance was related to a high PREN number for AL-6XN due to its high content of molybdenum and nitrogen. These results are consistent with existing literature on these alloys.
2. Windows of susceptibility based on electrochemical theories of corrosion were constructed for isolated AL-6XN in neutral sodium chloride solutions. This also demonstrated the intrinsic resistance of AL-6XN to crevice corrosion. The measured open circuit potential of isolated AL-6XN fell roughly 900 mV below the critical potential for crevice corrosion repassivation. This demonstrates that the "unsafe region" for crevice corrosion of isolated AL-6XN is far from the service potentials and conditions that would be expected in seawater in marine applications.
3. Isolated beads of complex multiphase Nicrobraz 31 was found to have unacceptable crevice corrosion resistance in marine environments when prepared at 1150°C for 60 minutes in a vacuum furnace. This lack of resistance was related to a low PREN number of the solid solution phase and the segregation of beneficial chromium due to the complex microstructure of the alloy in a bead form, representative of a joint of infinite clearance. The complex microstructure is a result of the formation of intermetallic compounds involving the melting point depressants (Si and P) in the braze alloy. It was suggested that a single-phase Nicrobraz 31 alloy would have improved corrosion resistance when compared to the multiphase form. However, even a single-phase specimen fabricated from Nicrobraz 31 would have a PRE number (22) far less than that for AL-6XN (45.7). The maximum joint clearance that would enable formation of a single phase Nicrobraz 31 would result was not clearly elucidated. However, a clearance below roughly 30 μm is implicated for wedge specimens of AL-6XN brazed with Nicrobraz 31 at 1150°C for 60 minutes.
4. Brazing AL-6XN with Nicrobraz 31 (1150°C/60 minutes) produced an extrinsic mode of crevice corrosion. From multiple crevice assembly tests in 6wt% FeCl_3 , the brazed alloy was attacked heavily on the brazed surface and not at all on the bare AL-6XN surface. The crevice corrosion attack greatly exceeded the thickness of the Nicrobraz 31 layer, indicating that AL-6XN had also been attacked. Through visual inspection of the specimen, it was observed that attack proceeded into the AL-6XN base metal via grain boundaries. These observations were duplicated after electrochemical experiments in the less aggressive solution of 0.6 M NaCl with neutral pH and minimal electrochemical polarization (0 to +100 mV_{SCE}). Specifically, at 0 mV, it was observed that the depth of attack was roughly 100 μm . This attack developed in 24 hours, indicating a rate of 100 $\mu\text{m/day}$. If a cellular panel is constructed with face sheets of about 2,500 μm thickness

the structure would be completely penetrated in 25 days. Furthermore, an open circuit potential of only 0 mV is very reasonable for stainless steel structures in marine environments.

5. The depassivation and lack of intrinsic crevice corrosion resistance of Nicrobraz 31 led to the development of a saturated nickel chloride solution, with low pH and high chloride content, in the occluded crevice environment. By electrochemical investigations, this harsh solution formed by initial corrosion of the Nicrobraz 31 alloy was found to depassivate and actively corrode AL-6XN. This confirms the mechanism of dissimilar metal crevice corrosion (DMCc) of AL-6XN in contact with Nicrobraz 31. The path of corrosion along the grain boundaries of AL-6XN was found to be due to Nicrobraz 31 penetration by wetting and solidification along the AL-6XN grain boundaries followed by dissimilar metal crevice corrosion. Attack of AL-6XN was not due to intrinsic sensitization of AL-6XN caused by the brazing thermal cycle.
6. A multiphase braze alloy was formed in all geometries of AL-6XN cellular structures brazed with Nicrobraz 31 (1150°C/60 minutes), indicating that a single phase Nicrobraz 31 is not easily obtained given the arrangement including possible large gaps in real sandwich structures. Therefore the multi-phase condition represents a true service situation. Additionally, the braze bead electrode was determined to be representative of the braze regions that were observed in the cellular panels. Corrosion initiation was observed in these multi-phase structures, consistent with electrochemical principles. However, extensive attack of cellular metal panels was not observed due to the lack of applied crevice sites during the ferric chloride and seawater exposure tests and shortage of exposure time.
7. The results listed above concerning the mechanistic aspects of Nicrobraz 31/AL-6XN corrosion would be applicable to any cellular metal topology, or design constructed of these materials. This is because similar gaps (diffusion lengths) would be expected to result in the same braze microstructure and dissimilar metal crevice corrosion in AL-6XN regardless of cell topology. It cannot be stated that any particular braze geometry would be better than another from this perspective for corrosion resistance, and the bottom line is that structures made of AL-6XN brazed with Nicrobraz 31 do not offer corrosion characteristics required for the proposed applications of cellular metals.

In summary, the following key guidance on corrosion mitigation was obtained.

1. The solid solution composition of an ideal solid solution braze alloy must be at least matched or overmatched with respect to the composition of good corrosion alloying elements typical of the super-austenitic stainless steel face sheet and core materials that it is intended to bond. The braze alloy should ideally provide an equal or higher pitting resistance equivalency number and critical pitting temperature.
2. The ideal solid solution form of the brazing alloying should be obtained by diffusion of melting point depressant from the braze material into the base material such that a single phase solid solution microstructure may be obtained. This enables the braze alloy to enjoy the fullest corrosion resistance possible. Narrow gap brazing clearances and post-braze heat treatment are recommended from the corrosion perspective.
3. The thermal cycle of the braze diffusion bonding process must not sensitize or produce detrimental phase formation in the superaustenitic stainless steel face sheet

and core materials such as Al-6XN nor should the alloy be susceptible to sensitization via formation of detrimental chromium phosphide phases formed by diffusion of the melting point depressant into the base material.

4. The melting point depressants present in the braze alloy should be potent enough to compensate for any elevation in melting temperature due to addition of alloying elements beneficial towards corrosion in order to preserve good brazing capability.

EDUCATIONAL SUMMARY

The research supported on a full-time basis one MS student who successfully obtained the MS degree in Materials Science and Engineering (Sara Anastasio) and lead to several oral and written presentations. Ms. Anastasio received a award at the International NACE CORROSION/05 Conference for the best engineering poster (Mars Fontana Award). Ms. Anastasio received her MS degree in July of 2005 [19]. Josh James is a second graduate student focusing on post-braze heat treatment and alloy design for good corrosion resistance. Josh started in the summer of 2005. The research also supported on a part-time basis two under-represented minorities in Engineering at UVA (Mr. Robert Amunfu), and Virginia Tech. (Ms. Jeannine Webb), a PDRA (Francisco Presuel) and a laboratory technician (Chris Marks). Several archival journal publications are in preparation based on this work.

RECOMMENDED FUTURE WORK

In order to develop joining technologies which optimize fabrication of cellular metal structures brazing alloys should be optimized and alternative joining strategies should be considered. The following critical questions must be addressed and present avenues for future work.

Braze structures:

- Can corrosion-metallurgy understanding of Microbraze type and other ferrous-based brazing alloys be exploited to develop intrinsic resistance to corrosion of brazed structures in harsh marine environments such as alternate and full immersion? What final composition associated with commercially available braze alloys containing controlled alloying additions designed to optimize corrosion performance will enable them to resist crevice corrosion in seawater and will extend the use of transient liquid phase bonded cellular metal structures to marine environments?
- What final composition associated with commercially available braze alloys containing controlled alloying additions designed to optimize corrosion performance will be compatible with super-austenitic stainless steels such as Al-6XN from the standpoint of mitigating susceptibility to dissimilar metal crevice corrosion (DMCc) ?
- What combinations of initial braze time-temperatures or follow up heat treatment time-temperature-diffusion length (e.g., core-face sheet gap) conditions enable formation of single phase solid solution braze microstructure microstructures capable of realizing the fullest potential for optimal corrosion resistance?

Welded structures:

- What are the crevice geometry, Cl^- potential, microstructure dependent windows of susceptibility for laser welded Al-6XN?
- What laser weld protocols optimize the corrosion resistance of laser welded SASS cellular metal structures?
- Can mechanistic insight as to local corrosion mechanisms of welds guided the proposition of mitigation strategies such as laser weld protocol, post-weld heat treatment and/or sacrificial cathodic prevention?

REFERENCES

1. Gibson, L.J. and M.F. Ashby, Cellular Solids Structure and Properties, Second edition. 1997: Cambridge University Press.
2. Wadley, H.N.G., Cellular Metals Manufacturing. Advanced Engineering Materials, 2002. 4(10): p. 726-733.
3. Evans, A.G., et al., The topological design of multifunctional cellular metals. Progress in Materials Science, 2001. 46: p. 309-327.
4. Wadley, H.N.G., N.A. Fleck, and A.G. Evans, Fabrication and Structural Performance of Periodic Cellular Metal Sandwich Structures. Composites Science and Technology, 2003. 63: p. 2331-2343.
5. A. Rider, "The Durability of Metal-Honeycomb Sandwich Structure Exposed to High Humidity Conditions," Defense Science and Technology Organization (Australia), pp. 1-102 (2002).
6. T.C. Radtke, A. Charon, and R. Vodicka, "Hot/Wet Environmental Degradation of Honeycomb Sandwich Structure Representative of F/A-18: Flatwise Tension Strength," Defense Science and Technology Organization (Australia), pp. 30 (1999).
7. J.R. Scully, "Corrosion of Cellular Metals in Marine Environments," SEAS Proposal No. MSE-DOD/NAVY/NSWC-098202, Dec. 2001.
8. Davison, R.M., T. DeBold, and M.J. Johnson, Corrosion of Stainless steels, Metals Handbook, 9th edition, volume 13, in Metals Handbook, 9th edition. 1987, ASM: Metals Park, OH. p. 547.
9. Grubb, J.F. and D.E. Deemer, AL-6XN Alloy (UNS N08367). 2002, Allegheny Ludlum Corporation: Pittsburg, PA. p. 54.
10. Grubb, J.F. Elevated Temperature Stability of a 6%Mo Superaustenitic Stainless Alloy, Paper No. 426. in NACE, 96. 1996: NACE.
11. Kearns, J.R., The Effect of Nitrogen on the Corrosion of Austenitic Stainless Steels Containing Molybdenum. Journal of Materials for Energy Systems, 1985. 7(1): p. 17.

12. A. John Sedriks, CORROSION OF STAINLESS STEELS, 2nd edition, Wiley-Interscience, John Wiley & Sons, Inc. (1996).
13. Kerns, J.R., M.J. Johnson, and J.F. Grubb. "Accelerated Corrosion in Dissimilar Metal Crevices" in Corrosion 86. 1986. Houston, Texas: NACE.
14. Sypeck, D.J. and H.N.G. Wadley, Cellular Metals and Metal Foaming Technology, ed. M.F.A. J. Banhart, N.A. Fleck. 2001: MIT-Verlag.
15. Wadley, H.N.G., N.A. Fleck, and A.G. Evans, Fabrication and Structural Performance of Periodic Cellular Metal Sandwich Structures. Composites Science and Technology, 2003. 63: p. 2331-2343.
16. Sypeck, D.J. and H.N.G. Wadley, Multifunctional microtruss laminates: Textile synthesis and properties. Journal of Materials Research, 2001. 16(3): p. 890-897.
17. Peaslee, R.L., Brazing Footprints; Case Studies in High-Temperature Brazing. 2003: Wall Colmonoy Corporation.
18. Ceccone, G. and M. Nicholas, The Brazing of Si_3N_4 with Ni-Cr-Si Alloys. Journal of European Ceramic Society, 1995. 15: p. pp. 563-572.
19. Sara L. Anastasio, "Corrosion Mechanisms in Brazed Cellular Stainless Steel Structures," A thesis presented to the Faculty of the School of Engineering and Applied Science, University of Virginia, July 2005.
20. Private communication, Dr. R.L. Peaslee and Amit Jain, Wall Colmonoy Corp., March, 2005.
21. Wolfe, C., T. Eklund, and O. Persson, Investigation of the corrosion performance of different braze fillers fused onto stainless steel type 1.4401 (UNS 31600), 2005, Alfa Laval/Sweden: Houston, TX.
22. Savage, E.I. and J.J. Kane, "Microstructural Characterization of Nickel Braze Joints as a Function of Thermal Exposure" Welding Journal, 1984. October 1984: p. 316-s.
23. Lugscheider, E. and K.D. Partz, High Temperature Brazing of Stainless Steel with Nickel-Base Filler Metals BNi-2, BNi-5 and BNi-7. Welding Journal, 1983. June 1983: p. 160s-164s.
24. R. Johnson, "The Use of TETIG Diagrams in High Temperature Brazing," Supplement to the Welding J., October 1981.

TECHNOLOGY TRANSFER

In FY2004-05 and the early part of FY2006, we established the mechanisms that govern the corrosion of a super-austenitic stainless steel Al-6XN (Fe-24Ni-20Cr-6.3Mo-0.22N) when brazed with a commercial Nicrobraz alloy (Nicrobraz 31: Ni-22Cr-6.3Si-3.8P) and exposed in a marine environment. This is a more scientific approach, as opposed to empirical corrosion studies that do not yield scientific information of generic and lasting value. We developed understanding that enables mitigation strategies to be proposed in three areas: (a) braze/superalloy post braze heat treatments and diffusion length combinations to optimize corrosion resistance, (b) sacrificial cathodic prevention of corrosion, (c) possible strategies for optimization of braze alloy composition to achieve better intrinsic corrosion resistance in a super-austenitic stainless steel Al-6XN (Fe-24Ni-20Cr-6.3Mo-0.22N) braze joint when brazed with a commercial Nicrobraz alloy.

Concerning option (a), heat treatment at 700 °C has been found to be beneficial and could be utilized in the marine application. Tests at 580 °C are not yet completed and are probably less of a risk of detrimental effects. Regarding option (b), we developed detailed information on cathodic prevention criteria that provides a basis for discussions with Navy engineers responsible for corrosion control via cathodic protection on ship structures. The information provided by this research can be input into fabrication methodologies and further large scale production of sandwich panels for trial application of mitigation of corrosion by strategy (a) or (b). The investigator is available to pursue either option or the concept may be transferred to US NAVY personnel consistent with this new knowledge base developed under this grant.

Regarding option (c), during FY2005 and 06, we developed substantial understanding of shortcomings of braze alloys and ways to improve the same. This work provides a basis for improved braze design. We have conducted discussions with both Allegheny Ludlum Steel Company (Mr. John Grubb) and Wall Colmonoy Corp. (Dr. Amit Jain and Dr. Bob Peaslee) concerning strategies to optimize braze compositions for improved intrinsic seawater corrosion resistance as well as improved dissimilar metal corrosion compatibility with Al-6XN in seawater service. The investigators have proposed this in a future proposal to ONR. Several new promising braze alloy compositions are ready to be attempted. Mr. Rick Wong at NSWC-CD is ready to be contacted regarding such braze alloy design. If these new alloys are developed, this technology should be transferred to optimize corrosion resistance of braze alloys for use with superaustenitic steels in seawater.

SUMMARY OF EXTERNAL DISSIMINATION OF FINDINGS

Contributed Presentations and Lectures

1. Sara Anatasio, John R. Scully, "Corrosion of Cellular Metals in Marine Environments," CORROSION/05, Student Poster Session, NACE, Houston, April, 2005.
2. Sara Anatasio, John R. Scully, "Corrosion of Cellular Metals in Marine Environments," Gordon Research Conference on Corrosion – Poster Session, July, 2004.
3. John R. Scully, Sara Anastasio, Joshua James, "Design of Corrosion Resistant Braze Alloys Optimized for Marine Application of Brazed Cellular Metal Structures," ONR Workshop in Multifunctional Cellular Materials and Structures, Airlie Virginia, August, 2005.
4. Joshua James, John R. Scully, "Corrosion Mitigation Strategies for Braze Superaustenitic Stainless Steel Cellular Metal Structures," Gordon Research Conference on Corrosion – Poster Session, July, 2006.

Invited Presentations and Lectures

1. John R. Scully, Sara Anastasio, "Corrosion of Cellular Materials in Marine Environments," ONR Workshop in Multifunctional Cellular Materials and Structures, Airlie, Virginia, September, 2004.

Publications

1. Corrosion of a super-austenitic stainless steel (Fe-24Ni-20Cr-6.3Mo-0.22N) when brazed with Nicrobraz 31 (Ni-22Cr-6.3Si-3.8P): Part I, Exposure studies, Journal of Corrosion Science and Technology, submitted (2005).
2. Corrosion of a super-austenitic stainless steel (Fe-24Ni-20Cr-6.3Mo-0.22N) when brazed with Nicrobraz 31 (Ni-22Cr-6.3Si-3.8P): Electrochemical Corrosion Behavior of Isolated and Combined Materials, Corrosion Journal, in preparation, (2005).
3. Corrosion of a super-austenitic stainless steel (Fe-24Ni-20Cr-6.3Mo-0.22N) when brazed with Nicrobraz 31 (Ni-22Cr-6.3Si-3.8P): Dissimilar Metal Crevice Corrosion Mechanism in SASS, Corrosion Journal, in preparation, (2005).
4. J. James, J.R. Scully, "Effect of Brazing Diffusion Length on Corrosion of a Super-Austenitic Stainless Steel (Fe-24Ni-20Cr-6.3Mo-0.22N) brazed with Nicrobraz 31 (Ni-22Cr-6.3Si-3.8P), Corrosion Journal, in preparation, (2006).

Chapters/Books (September, 2004- August, 2006)

1. J.R. Scully, Chapter on **Electrochemical Methods in Laboratory Corrosion Testing**, in **ASTM Manual on Corrosion Tests and Standards, Application and Interpretation 2nd ed.**, ASTM West Conshohoken, PA, pp. 107-130, (2005).

2. J.R. Scully, R.G. Kelly, Chapter on **Electrochemical Methods in Laboratory Corrosion Testing**, in ASM Metals Handbook, Vol. 13A, CORROSION, Fundamental, Testing and Protection, pp. 68-80, ASM, Metals Park OH (2005).

Honors (2004-2006)

1. Sara A. Anastasio, NACE Intl. CORROSION/05 Conference Poster Session, Poster Award, Harvey Herro Technology Division, 1st Place, 2005.
2. John R. Scully: Francis LaQue Award for Achievements in Corrosion Science and Engineering, November 2005.
3. John R. Scully: Elected Fellow of the Society, The Electrochemical Society, October 2005.

Patents

None